Earl Nick (Orcid ID: 0000-0002-6375-0699)
Simmonds Ian (Orcid ID: 0000-0002-4479-3255)

Sub-synoptic-scale features associated with extreme surface gusts during the South Australia Storm of September 2016 – Part I: Characteristics of the event

Nick Earl*[1,2], Ian Simmonds[1] and Irina Rudeva[1]

[1] School of Earth Sciences, The University of Melbourne, Parkville, Melbourne, Victoria, 3010, Australia.

[2] Institute for Marine and Antarctic Studies, The University of Tasmania, Hobart, Tasmania, 7003, Australia.

*corresponding author – nearl@unimelb.edu.au

Abstract

Winds are one of the major contributors to deaths, damage and insured losses in Australia. A 'freak storm', which left 1.7 million people without power, hit the state of South Australia on the 28th September 2016, causing state-wide blackouts. In the first part of this two part study, we analyse this event and find that it was indeed extreme, deepening more explosively than all but two Adelaide-affecting extra-tropical cyclones over the past 37 years and exhibiting the lowest central pressure. This generated hurricane force winds, with central South Australia site of Neptune Island recording a gust of over 120kmh^{-1}. We show that this storm potentially contained a sting jet. Such jets are well known to cause major damage over Europe, and this is the first study which investigates whether a sting jet can be produced over Australia. The main deepening of the system occurred over the Great Australian Bight, so if a sting jet did form and make it to the surface, it was not the cause of

This is the author manuscript accepted for publication and has undergone full peer review but has not been through the copyediting, typesetting, pagination and proofreading process, which may lead to differences between this version and the Version of Record. Please cite this article as doi: 10.1002/wea.3385

the state-wide damage. However, the cyclone did contain numerous extreme gust-producing mesoscale features as explored in part II of this paper.

Introduction

Extreme winds are one of the major contributors to deaths, damage and insured losses in many parts of the world. In Australia, these occur on a wide range of spatial scales throughout the continent, yet we poorly understand the diverse and variable causal processes. Systems associated with these winds include fronts, downbursts and tornadoes from supercells or bow echoes, tropical cyclone (TC) and extratropical cyclone (ETC) development. These are more or less dominant in different parts of Australia, with TCs affecting the northern regions and ETCs causing damage and destruction in the south. For example, the wind contributed to the US$1 billion loss from TC Oswald of 2013 and the US$0.9 billion loss from the Brisbane storm of November 2014 (Swiss Re 2017). As to ETCs a notable example of these occurred off New South Wales in June 2007. It caused severe wind and rain damage, resulting in 10 deaths, and insurance claims of around US$1.3 billion, making it one of the most costly natural disasters in Australia's history (Mills *et al. 20*10). ETCs differ from TCs in that they are driven by the contrast in temperatures in the mid-latitudes, and hence only affect the southern states and also possess many different features which cause surface gusts. These include frontal systems, which move from west to east along the Southern Ocean polar front and East Coast Lows which develop off the east

coast of New South Wales and Victoria, driven by a complex combination of baroclinicity and conducive atmospheric background conditions (Chambers *et al*. 2014, 2015). Polar front ETCs commonly affect the southern states of Australia during winter, but not so much during summer. These storm tracks have been found to be shifting southwards in the warming climate (Frederiksen and Frederiksen 2007; Pezza *et al. 20*07; Rudeva and Simmonds 2015) However they still produce damaging winds when they affect Australia.

On the 28th September, an extreme ETC (hereafter ETC28) impacted the state of South Australia causing state-wide blackouts and damage. The Australian Bureau of Meteorology (BoM) describes the synoptic scale development of ETC28 from the time of affecting south-west Western Australia on the 27th (BoM 2016). For similar ETC events over the UK, Earl *et al.* (2017) highlighted the many mesoscale features which produce extreme surface winds varying greatly in gust severity, frequency, swath and position relative to the low pressure centre. We provide comprehensive analysis of ETC28 in a two-part paper. Here, we ascertain the extent to which the ETC track and its development were unusual and also put the ETC into longer term context by analysing the gusts compared to previous events detected by the surface station network. We also determine whether ETC28 is a candidate for containing a Sting Jet (Browning 2004), by analysing the ETC's development. Wind direction is also very important with regard to insured losses (Khanduri and Morrow 2003). Anecdotal reports suggest, for example, an ETC event in February 2005 was especially

damaging (relative to the wind speeds observed) in Melbourne and northern Tasmania because the winds were easterly, a rare direction for strong winds in the region. This paper includes wind direction in feature identification and can also give insights into potential damage. In part II we highlight which aspects of the ETC caused the most severe surface wind gusts, and to establish whether Australian ETCs exhibit similar behaviours to their western Europe counterparts. This is the first southern hemisphere ETC to be split into different sub-synoptic scale features in this way, with its extremity based on surface wind observations.

Extra-tropical cyclones

Research into the structure of ETCs has a rich history, since the development of the first conceptualised ETC life-cycle model, the Norwegian cyclone model, developed at the Bergen Geophysical Institute in the late 1910s. It located cyclogenesis along the Northern Hemisphere polar front and dividing the cycle into stages of the typical life of a low pressure system in the extra-tropics (e.g. Parton *et al. 20*10). This formed the basis for the conveyor belt paradigm of Browning (1971) and the development of the Shapiro and Keyser (1990) cyclone model (Figure 1). Not all explosively deepening ETCs follow the Shapiro-Keyser conceptual model life cycle. It is dependent on whether the ETC is embedded in diffluent or confluent large-scale flow in the upper-levels, with the former producing ETCs more likely to follow the Norwegian life-cycle model (see Schultz *et al., 1*998). Schultz and Vaughan (2011)

provided a modified view of the occlusion front paradigm within the Norwegian cyclone model suggesting that the occlusion process is the ETC as wrapping-up (differential rotation further from the ETC centre) rather than the cold front catching-up the warm front. Their approach resolved anomalies within the conceptual model and provides a better and more general fluid-dynamical description of the occlusion process.

Sting jet

During the passage of ETCs over western European, Browning (2004) highlighted that the most extreme surface winds were due to a mesoscale feature at the tip of the cloud head known as a Sting Jet (SJ). These are a short lived (a few hours), mesoscale features associated with strong evaporation at the tip of the cloud head hook, enhancing the dry slot windspeeds, dubbed the 'sting in the tail' (Browning 2004; Clark et al. 2005). Latent heat used during the evaporation of cloud droplets and rainfall within this region of slantwise descent results in strong gusts that can reach the surface, though some researchers have described cases in which moist processes were not important (e.g. Schultz and Sienkiewicz 2013; Baker et al 2014; Smart and Browning 2014; Slater et al. 2015). Conditional symmetric instability (Gray et al. 2011) in, and upwind of, the dry slot region can produce mesoscale slantwise circulations, also contributing to the severity of the SJ. This was proven to be the case for the UK '16th October 1987 Storm' (Clark *et al. 20*05), ETC Jeanette in October 2002 (Parton *et al. 20*09), ETC Christian in October 2013 (Browning *et al. 20*15) and others.

Martínez-Alvarado *et al.* (2012) suggested that SJs are a generic feature of ETCs occurring in between 23 and 32% of the strongest ETCs affecting western Europe. Furthermore, recent work by Martínez-Alvarado et al (2018) found that the proportion of ETCs with a proven SJ precursor (midtropospheric atmospheric instability to slantwise descent diagnosed using downdraught slantwise convective available potential energy) increases to 45% in a future warmer climate. There is no study in the literature that examines whether SJs occur over the Australian continent, despite the southern part of this region experiencing European-like ETCs especially during winter and could become more influential in the future.

28th-30th September 2016 South Australia ETC

ETC28 was one of the most significant Australian ETC events in recent decades. Despite the BoM surface pressure charts resembling the Norwegian model (Figure 2), our analysis concludes that it closely followed the Shapiro-Keyser model, with a bent back cloud head and frontal fracture visible in the satellite images (Figure 3). The Shapiro-Keyser model was developed for eastern Atlantic Ocean and western European ETCs, but apply broadly to marine extratropical cyclones in the Australian region (Sinclair and Revell 2000), with a bent back cloud head and frontal fracture from the low-pressure-centre as it developed. The 28th saw damaging winds, leading to a South Australia-wide blackout. A total of 23 pylons on electricity transmission lines were damaged, including three of the four interconnectors

connecting the Adelaide area to the north and west of the state, leading to cascading failure of the electricity transmission network.

Early on the 27th, an upper level trough became 'cut off' from the polar jet as it travelled east, entering South Australia. This resulted in a transfer of vorticity to the surface, driving explosive deepening of ETC28 in the Great Australian Bight. The synoptic charts (Figure 2) and satellite images (Figure 3) suggests frontal fracture occurring around 0000 UTC on the 28th and the bent back cloud head clearly visible at 0500 UTC. The central pressure fell 23 hPa (according to the BoM) in 24 hours from 0600 UTC on the 27th to 0600 to be 973 hPa on the 28th as highlighted in Figure 2. Once corrected to 60° latitude (sin Φ/sin60), this deepening of over 1 Bergeron is considered a 'bomb' in the terminology of Sanders and Gyakum (1980). Lim and Simmonds (2002) have generalised this criterion to take into account the change in climatological mean sea level pressure (SLP) as the cyclone moves into different regions. This is known to be an important factor in the southern hemisphere which is characterised by strong meridional gradients of SLP. However, the motion of ETC28 was predominantly zonal, and the storm still qualified as an 'explosive developer' even with this more restrictive definition.

The explosive development occurred in the Great Australian Bight and the ETC centre did not reach landfall until well into stage IV of its life cycle around 0000 UTC on the 29th.

'Supercell thunderstorms' formed along the cold front causing the destructive winds, with 'at least seven tornadoes', hail and very intense rain on the 28th (BoM 2016). Much research, as reviewed by Schenkman and Xue (2016), has focused on mesovorcites and tornadoes forming along convective lines (explored in part II), so this is likely to be the case for ETC28. These affected a vast swath of South Australia and caused considerable damage, including widespread power outages. The preceding months were very wet in South Australia and this moisture excess was enhanced by precipitation along a trough in front of the cold front a few hours prior to the cold front. Clear skies led to strong surface heating after this precipitation, which had raised the dew point temperatures and convective available potential energy, all contributing to this development along the cold front, together with the temperature contrast behind the front. Our analysis explores how the large scale pattern set itself in the days prior to the event, and does this, in part, by using a cyclone-tracking algorithm to determine the origin and evolution of the storm.

Data and methods

Data

Reanalysis data utilised in this study are from the European Centre for Medium-Range Weather Forecasts Reanalysis (ERA)-Interim (Dee *et al. 20*11) project at 6-hour and 0.5˚ latitude-longitude resolution (1979-2016). Surface wind gust speed and direction observations are taken from the BoM website (datasets ranging from 1939-present to 2015-

present (see Table 1)). BoM 6 hourly synoptic charts and 10 minute radar precipitation rate images are also used. Satellite imagery is from the geostationary Himawari platform at 10 minute temporal resolution. These high temporal resolution datasets (especially the radar, available here http://www.theweatherchaser.com/radar-loop/IDR643-adelaide-buckland-park/2016-09-28-04/2016-09-29-04) are crucial, allowing us to observe the exact location of the ETC features, from their precipitation signals.

Methods

ETC tracks are identified using the scheme developed at the University of Melbourne and described in Simmonds and Keay (2002) and Keable *et al.* (2002). The algorithm objectively identifies and tracks cyclones at 6-hourly intervals based on the structure of SLP fields derived from the ERA-Interim reanalysis. This scheme has been used in a range of analyses of cyclone activity in both hemispheres and its results are in good agreement with other methods used for cyclone identification and tracking (e.g. Pinto *et al. 20*05; Raible *et al. 20*08; Simmonds *et al. 20*08; Neu *et al. 20*13).

The daily maximum gust speeds (DMGSs) are ranked in order of intensity for each of the 61 BoM operational observational network sites (Figure 4) for all available data. With the wide-range of site operational lifetimes, we highlight the length of record at each site in Table 1

and when mentioned in the text. DMGSs reaching the top 5%, 1% and 0.1% (hereafter, 5DMGS, 1DMGS and 0.1DMGS; based on number of data points rather than lifetime because of data dropouts) during the 28th, 29th and 30th September 2016 are highlighted at each site (following the method of Earl *et al.* (2017)). During the development of a windstorm loss model, Hewston (2008) highlighted that it was the top 2% of local DMGSs at specific locations, rather than the absolute wind speeds themselves, that resulted in most damage to UK insured property. Concentrating here mainly on the 1DMGSs and 0.1DMGSs therefore places specific emphasis on the most damaging and life-threatening winds, with the 5DMGSs providing additional information.

Results and discussion

Storm track

Track analysis highlights that ETC28 formed over the southern Indian Ocean on the 26th September and reached South Australia two days later (Figure 2). To put this into a climatological perspective we analysed all ETCs (1979-2016) that had similar trajectories, namely generated over the South Indian Ocean (east of 120°E and south of 35°S) and then moved across a 5˚x 5˚ (136.5-141.5°E, 32.5-37.5°S) box centred over Adelaide. Some ETCs reach Adelaide from the continent (not shown), however, we are only interested in ETCs that have a similar track to ETC28. We found 182 other ETCs that followed a similar trajectory, and tend to occur during the cooler months including September (Figure 5).

Of the 183 tracks, ETC28 had the lowest SLP in the cyclone centre when it moved across Adelaide (Figure 5). Our tracking analysis shows that It possessed the third fastest 24-hour deepening, 21.2hPa and, after latitude normalization (Sanders and Gyakum, 1980), is rated as an 'explosive developer' (1.24 Bergeron). This shows that ETC28 was an extreme ETC for this area, a one in ten year event, with comparable ETCs usually tracking further south (Lim and Simmonds 2002). In the following two sub-sections we explore the surface wind association with this intense ETC, and determine where and why the strongest gusts occurred.

Strongest gust locations

Figure 6 displays the locations of observed surface gusts for each day ETC28 was affecting South Australia (also displayed in Table 1). The 28th and 29th both experienced multiple extreme gusts, whereas by the 30th ETC28 had weakened over South Australia.

28th September

On the 28th, the sites which experienced the strongest winds were spread throughout the state, however the Adelaide Metropolitan area was spared any 1DMGSs. Numerous sites experienced amongst their strongest ever gusts, for example the most western South Australia BoM site, Nullarbor (Figure 4) experienced the 2nd strongest gust (27.8 ms^{-1}; see

Table 1 for all gust rankings) in its 28-year history and Leigh Creek (26.2 ms^{-1}), in east South Australia (800km east of Nullarbor), recorded its 6th strongest gust its 34-year history. Of the 55 BoM sites which recorded DMGSs that day (some dropped out perhaps due to the wind), the strongest was 31.4 ms^{-1} at Yunta airstrip and was the strongest gust ever recorded here in its 13 years of recording. The times of the 0.1DMGSs are displayed in Table S1, which highlights the wide ranging times of 0.1DMGSs experienced at each site, for example the gust at Leigh Creek occurred at 20:19 ACST, but Yunta (300km SSE) occurred 2:30hrs earlier at 17:50 ACST. When examined in more detail with satellite/radar and synoptic charts (Figures 2 and 3), it is clear that the Yunta gust occurred as the cold front moved over the site, however the Leigh Creek site occurred far behind the front (discussed below in part II). It is noteworthy that some sites located near those mentioned above did not produce even a 1 in 20 day (or top 5%) gust. Coastal sites Cape Jaffa (19 ms^{-1}) and Robe Airfield (18 ms^{-1}) DGMSs were outside the 5th percentile, whereas Coonawarra, just 100km inland produced the 5th strongest gust (24.7 ms^{-1}) in its 15-year history. This highlights the fact that wind producing features within storms vary greatly spatially. Also, some sites usually sheltered from the prevailing south-westerly wind are more exposed from other directions. However, DMGSs were mainly northerly the 28th (see Table S1 for gust direction), which is a common wind direction according to the BoM (http://www.bom.gov.au/climate/averages/wind/selection_map.shtml). Therefore, the orientation of the DMGSs were unlikely to have contributed to the widespread damage to transmission lines, leading to the state-wide blackout on the 28th. Many of the damaged

transmission lines were in the Port Augusta area (Figure 4; central South Australia, 300 km north of Adelaide), and this site experienced a 1DMGS from the NNE.

2) *29th September*

On the 29th, the low-pressure-centre tracked just south of Adelaide metropolitan area. This brought 1DMGSs to the central part of South Australia, while the far north and southeast were unaffected. The pattern of DMGS percentiles is less sporadic than the previous day, with the grouping together of similar severity of DMGSs. The strongest South Australia DMGS recorded throughout ETC28 occurred on the exposed Neptune Island, 33.4 ms^{-1}, the 4th strongest DMGS seen since recording began in January 1985. The coastal Ceduna site in western South Australia clocked the 2nd strongest DMGS, 31.9 ms^{-1}, the 10th strongest gust of its 76-year history, with its neighbour, Thevenard not recording, possibly due to damage. Figure 6 shows how many sites experienced 0.1DMGSs and 1DMGSs on the perhaps less infamous 29th September (compared with the 28th) with numerous 1DMGSs affecting the Adelaide metropolitan area. The timing of most 1DMGSs affected the surface sites in the vicinity of the low-pressure-centre as it migrated eastward.

30th September

The ETC was moving off eastward on the 30th with just a handful of 5DMGSs. The severity of DMGSs affecting the Adelaide area was comparable to the 28th. There were no 1DMGSs recorded on the 30th, but Edinburgh RAAF site recorded a top 2% gust which occurred along the occluded front, as the main system past.

Sting jet

Explosive deepening of an ETC is one of the main contributing factors towards the formation of sting jets within them (Browning 2004). The main development occurred offshore and the ETC centre did not make landfall until well into stage IV of its life cycle around 0000 UTC on the 29th. This means that it is very unlikely that any extreme winds experienced during ETC28 were caused by a SJ (only seen in stages II and III of the Shapiro-Keyser life cycle model) and that other mechanisms were responsible for the extreme surface winds as explored in part II. If a SJ did form and reach the surface, this is likely to have occurred in the Great Australian Bight but certainly did not make landfall. However, as mentioned, ETC28 deepened explosively and had a clear bent back cloud head with likely evaporation at the tip of the cloud head hook, seen on the 28th (Figure 3). As SJs are likely to be a generic feature of ETCs (Martínez-Alvarado *et al. 20*12), ETC28 looks likely to have contained one. However, the lack of observations makes it impossible to prove without modelling (by following the method of Smart and Browning (2014)), which is outside the scope of this paper. With SJs

predicted to be more influential in the future (Martínez-Alvarado *et al.* 2018) the study of Australian SJ is imperative.

Conclusions

ETCs commonly affect southern Australia and ETC28 was an extreme among these. The storm was one of the most intense storms to hit the state of South Australia in recent decades, and left millions without power and brought the state to a standstill. This region is prone to ETCs and the question was raised as to why this particular ETC was so damaging, described anecdotally as a 1 in 50 year event? What were the specific characteristics that created such severe surface winds? The ETC progressed along a prevalent track and followed the Shapiro-Keyser life cycle model common in European explosive ETCs. However, of these similar-tracking ETCs, the ETC28 low pressure centre deepened more explosively than all but two over the past 37 years and reached the lowest central pressure of all. With this explosive development, ETC28 potentially contained a SJ, however this deepening occurred offshore, so if a SJ made it to the surface, it was not the cause of the state-wide damage. The storm contained numerous extreme gust-producing mesoscale features as explored in part II of this paper.

Acknowledgements

Parts of this research were made possible by funding from the Australian Research Council (ARC) Grant DP16010997. Nick Earl was also supported by the ARC (CE110001028).

References

Atkins NT, Bouchard CS, Przybylinski RW, Trapp RJ, Schmocker G. 2005. Damaging surface wind mechanisms within the 10 June 2003 Saint Louis bow echo during BAMEX. *Mon. Weather. Rev.*, 133(8): 2275-2296

Baker LH, Gray SL, Clark PA. 2014. Idealised simulations of sting-jet cyclones. *Q. J. R. Meteorol. Soc.* 140: 96–110.

Browning KA. 1971. Radar measurements of air motion near fronts. *Weather*. 26(8): 320-340.

Browning KA. 2004. The sting at the end of the tail: Damaging winds associated with extratropical cyclones. *Q. J. R. Meteorol. Soc.* 130: 375-399. doi: 10.1256/qj.02.143.

Browning KA, Smart DJ, Clark MR, Illingworth AJ. 2015. The role of evaporating showers in the transfer of sting-jet momentum to the surface. *Q. J. R. Meteorol. Soc.* 141: 2956–2971. doi.org/10.1002/qj.2581.

Bureau of Meteorology. 2016. Severe thunderstorm and tornado outbreak South Australia 28 September 2016. 54 pp. http://www.bom.gov.au/announcements/sevwx/sa/Severe_Thunderstorm_and_Tornado_Outbreak_28_September_2016.pdf.

Chambers, C. R. S., Brassington, G. B., Simmonds, I. and Walsh, K. 2014. 'Precipitation changes due to the introduction of eddy-resolved sea surface temperatures into simulations of the "Pasha Bulker" Australian east coast low of June 2007', *Meteorol. Atmos. Phys*., 125, 1-15, doi: 10.1007/s00703-014-0318-4.

Chambers, C. R. S., Brassington, G. B., Walsh, K. and Simmonds, I. 2015. 'Sensitivity of the distribution of thunderstorms to sea surface temperatures in four Australian east coast lows', *Meteorol. Atmos. Phys*., 127, 499-517, doi: 10.1007/s00703-015-0382-4.

Clark PA, Browning KA, Wang C. 2005. The sting at the end of the tail: Model diagnostics of fine-scale three-dimensional structure of the cloud head. *Q. J. R. Meteorol. Soc.* 131(610): 2263-2292.

Dee DP, Uppala SM, Simmons AJ, Berrisford P, Poli P, Kobayashi S, Andrae U, Balmaseda MA, Balsamo G, Bauer P, Bechtold P. 2011. The ERA-Interim reanalysis: Configuration and performance of the data assimilation system. *Q. J. R. Meteorol. Soc.* 137(656): 553-597.

Earl N, Dorling S, Starks M, Finch R. 2017. Subsynoptic-scale features associated with extreme surface gusts in UK extratropical cyclone events. *Geophys. Res. Lett.* 44: 3932–3940. doi:10.1002/2017GL073124.

Frederiksen JS, Frederiksen CS. 2011. Twentieth century winter changes in Southern Hemisphere synoptic weather modes. *Adv. Meteorol.* 353829. doi: 10.1155/2011/353829.

Gray SL, Martínez-Alvarado O, Baker LH, Clark PA. 2011. Conditional symmetric instability in sting-jet storms. *Q. J. R. Meteorol. Soc.* 137(659): 1482-1500.

Hewston R. 2008. Weather, climate and the insurance sector. Ph.D. dissertation, University of East Anglia; 312 pp.

Keable M, Simmonds I, Keay K. 2002. Distribution and temporal variability of 500 hPa cyclone characteristics in the Southern Hemisphere. *Int. J. Climatol.* 22: 131-150.

Khanduri AC, Morrow GC. 2003. Vulnerability of buildings to windstorms and insurance loss estimation. *J. Wind Eng. Ind. Aerod.* 91(4): 455-467.

Lim EP, Simmonds I. 2002. Explosive cyclone development in the Southern Hemisphere and a comparison with Northern Hemisphere events. *Mon. Weather. Rev.* 130: 2188-2209.

Martínez-Alvarado O, Gray SL, Catto JL, Clark PA. 2012. Sting jets in intense winter North-Atlantic windstorms. *Environ. Res. Lett.* 7: 024014.

Martínez-Alvarado O, Gray SL, Hart NC, Clark PA, Hodges K, Roberts MJ. 2018. Increased wind risk from sting-jet windstorms with climate change. *Environ. Res. Lett.* 13: 044002.

Mills GA, Webb R, Davidson NE, Kepert J, Seed A, Abbs D. 2010. The Pasha Bulker east coast low of 8 June 2007. Centre for Australia Weather and Climate Research Tech. Rep. 23, 62 pp. [Available online at http://www.cawcr.gov.au/publications/technicalreports.php.]

Neu U, Akperov MG, Bellenbaum N, Benestad R, Blender R, Caballero R, Cocozza A, Dacre HF, Feng Y, Fraedrich K, Grieger J. 2013. IMILAST: A community effort to intercompare extratropical cyclone detection and tracking algorithms. *Bull. Am. Meteorol. Soc.* 94: 529-547. doi: 10.1175/BAMS-D-11-00154.1

Parton GA, Vaughan G, Norton EG, Browning KA, Clark PA. 2009. Wind profiler observations of a sting jet. *Q. J. R. Meteorol. Soc.* 135(640): 663-680.

Parton G, Dore A, Vaughan G. 2010. A climatology of midtropospheric mesoscale strong wind events as observed by the MST radar, Aberystwyth. *Meteorol. Appl.* 17: 340–354. doi:10.1002/met.203.

Pezza AB, Simmonds I, Renwick JA. 2007. Southern Hemisphere cyclones and anticyclones: Recent trends and links with decadal variability in the Pacific Ocean. *Int. J. Climatol.* 27: 1403-1419. doi: 10.1002/joc.1477.

Pinto JG, Spangehl T, Ulbrich U, Speth P. 2005. Sensitivities of a cyclone detection and tracking algorithm: Individual tracks and climatology. *Meteorol. Z*. 14 : 823–838.

Raible CC, Della-Marta PM, Schwierz C, Wernli H, Blender R. 2008. Northern Hemisphere extra-tropical cyclones: A comparison of detection and tracking methods and different reanalyses. *Mon. Wea . Rev.*136: 880–897.

Rudeva I, Simmonds I. 2015. Variability and trends of global atmospheric frontal activity and links with large-scale modes of variability. *J. Clim.* 28: 3311-3330.

Sanders F, Gyakum JR. 1980. Synoptic-dynamic climatology of the “bomb”. *Mon. Weather. Rev.* 108: 1589-1606.

Schenkman AD, Xue M. 2016. Bow-echo mesovortices: A review. *Atmos. Res.* 170: 1-13. doi: 10.1016/j.atmosres.2015.11.003

Schultz DM, Keyser D, Bosart LF. 1998. The effect of largescale flow on low-level frontal structure and evolution in midlatitude cyclones. *Mon. Weather. Rev.* 126: 1767–1791.

Schultz DM, Vaughan G. 2011. Occluded fronts and the occlusion process: A fresh look at conventional wisdom. *Bull. Am. Meteorol. Soc.* 92: 443–466 ES19–ES20.

Schultz DM, Sienkiewicz JM. 2013. Using frontogenesis to identify possible sting jets in extratropical cyclones. *Weather Forecasting.* 28: 603–613.

Shapiro MA, Keyser DA. 1990. Fronts, jet streams, and the tropopause. *Extratropical Cyclones: The Erik Palmén Memorial Volume*, C. W. Newton and E. O. Holopainen, Eds*. Am. Meteorol. Soc.* 167–191.

Simmonds I, Burke C, Keay K. 2008. Arctic climate change as manifest in cyclone behavior. *J. Clim.* 21: 5777-5796. doi: 10.1175/2008JCLI2366.1.

Simmonds I, Keay K. 2002. Surface fluxes of momentum and mechanical energy over the North Pacific and North Atlantic Oceans. *Meteorol. Atmos. Phys.* 80: 1-18. doi: 10.1007/s007030200009.

Sinclair MR, Revell MJ. 2000. Classification and composite diagnosis of extratropical cyclogenesis events in the southwest Pacific. *Mon. Weather. Rev.* 128(4): 1089-1105.

Slater TP, Schultz DM, Vaughan G. 2015. Acceleration of near-surface strong winds in a dry, idealized extratropical cyclone. *Q. J. R. Meteorol. Soc.* 141: 1004–1016. doi:10.1002/qj.2417

Smart DJ, Browning KA. 2014. Attribution of strong winds to a cold conveyor belt and sting jet. *Q. J. R. Meteorol. Soc.* 140: 595–610

BoM Site number	Start date	Gust speed 28th (ms^{-1})	Gust rank 28th (top%)	Gust speed 29th (ms^{-1})	Gust rank 29th	Gust speed 30th (ms^{-1})	Gust rank 30th
16001	May 1949	26.7	98(0.5%)	25.2	144(0.7%)	17	2365(11.3%)
16090	Mar 2004	24.2	37(0.8%)	23.1	54(1.2%)	15.4	895(19.1%)
16096	Mar 2007	25.7	4(0.1%)	21.1	25(0.7%)	13.9	650(18.5%)
16097	May 2003	22.1	28(0.6%)	17	272(5.7%)	10.8	2467(51.8%)
16098	Aug 1999	25.7	5(0.1%)	23.7	17(0.3%)	13.4	1279(25.4%)
17043	Mar 1941	25.2	157(0.8%)	19.5	1019(4.9%)	13.9	5261(25.4%)
17110	May 1982	26.2	6(0.1%)	20.6	80(1.6%)	20.6	80(1.6%)
17123	Apr 2005	19.5	57(1.4%)	18	124(2.9%)	12.9	1019(24.1%)
17126	Apr 2003	24.2	40(0.8%)	23.1	53(1.1%)	13.4	1476(30.5%)
18012	Mar 1940	24.7	191(0.7%)	31.9	10(0%)	15.9	5200(19%)
18083	Aug 2003	27.3	6(0.1%)	22.1	47(1%)	14.9	826(17.2%)
18106	Jan 1988	27.8	2(0.1%)	22.1	42(1%)	9.3	3439(85.7%)
18115	Jan 1985	26.7	127(2.7%)	33.4	4(0.1%)	25.2	193(4%)
18116	Jul 2003	N/A	N/A	24.7	26(0.5%)	13.9	1406(29.2%)
18120	Sep 2003	24.2	13(0.3%)	22.6	37(0.8%)	14.9	976(20.4%)
18191	Aug 2003	27.8	7(0.2%)	29.3	3(0.1%)	18	254(5.6%)

18192	Aug 2003	26.7	10(0.2%)	29.8	4(0.1%)	15.4	790(16.6%)
18195	Aug 2003	23.1	15(0.3%)	24.7	5(0.1%)	11.3	2365(49.5%)
18200	Mar 2015	27.8	1(0.1%)	N/A	N/A	18.5	51(7.1%)
18201	Aug 2003	24.7	16(0.4%)	26.2	10(0.2%)	17	379(9.4%)
20062	Jun 2003	31.4	1(0%)	24.2	28(0.6%)	18.5	223(4.6%)
21131	Jul 2003	16.5	174(3.6%)	22.1	5(0.1%)	17.5	100(2%)
21133	Oct 2003	28.8	3(0.1%)	25.2	17(0.4%)	21.1	111(2.3%)
21139	Jan 2015	26.7	1(0.1%)	24.2	5(0.7%)	18	38(5.1%)
22031	Aug 2003	25.2	26(0.5%)	26.7	12(0.2%)	19	306(6.2%)
22046	Jul 1984	20.6	145(2.9%)	23.7	48(1%)	15.4	750(15.2%)
22049	Jul 2003	22.6	85(1.7%)	28.3	2(0%)	17	631(12.8%)
22050	Jul 2005	22.6	47(1.1%)	28.8	1(0%)	20.6	110(2.6%)
22053	Jul 2003	24.2	20(0.9%)	N/A	N/A	21.6	64(2.8%)
22803	Jun 2000	27.3	69(1.6%)	28.3	42(1%)	20.6	538(12.7%)
22823	Feb 2004	20.1	277(6.1%)	27.8	9(0.2%)	17	667(14.7%)
22841	Oct 2003	21.6	48(1%)	23.1	19(0.4%)	16.5	398(8.3%)
22843	Sep 2011	22.6	22(1.1%)	24.7	8(0.4%)	15.9	221(11.1%)
23013	Jul 1939	19	1000(6.2%)	21.6	440(2.7%)	18.5	1208(7.5%)
23034	Feb 1955	21.1	581(2.6%)	23.1	317(1.4%)	17	2135(9.5%)
23052	Mar 2015	23.7	8(1.1%)	26.7	2(0.3%)	22.1	15(2.1%)
23083	Jan 1973	20.6	381(2.9%)	24.7	81(0.6%)	22.1	208(1.6%)
23090	Feb 1977	13.9	1991(13.8%)	19	239(1.7%)	13.9	1991(13.8%)
23109	Oct 2011	N/A	N/A	23.1	7(0.4%)	14.9	166(8.4%)
23122	Aug 1997	17.5	335(6.6%)	24.2	17(0.3%)	19.5	154(3%)
23123	Oct 2011	N/A	N/A	22.6	5(0.3%)	17.5	59(3.1%)
23124	Sep 2011	19	47(2.4%)	22.6	12(0.6%)	16.5	130(6.6%)
23373	Jul 2004	18.5	163(3.6%)	23.1	13(0.3%)	19.5	102(2.3%)
23842	Sep 2004	17.5	380(8.8%)	22.1	60(1.4%)	13.9	942(21.9%)
23875	Jul 2004	17	328(7.2%)	22.6	28(0.6%)	13.9	966(21.2%)
23878	Jun 2004	25.2	51(1.1%)	27.3	18(0.4%)	20.6	256(5.6%)
23885	Apr 2004	N/A	N/A	21.1	46(1%)	14.9	731(15.6%)
23886	Sep 2011	19	108(5.4%)	20.1	65(3.3%)	12.3	851(42.9%)
23887	Aug 2003	17	426(8.7%)	23.1	33(0.7%)	17	426(8.7%)
24024	Nov 1998	17.5	152(2.3%)	19.5	56(0.9%)	14.9	448(6.9%)
24048	Dec 2003	N/A	N/A	20.6	80(1.7%)	17	309(6.5%)
24580	Mar 2004	18.5	287(6.1%)	20.1	165(3.5%)	17.5	390(8.2%)
24584	Mar 2006	17.5	267(6.8%)	19	142(3.6%)	18.5	183(4.7%)
25557	Sep 2004	23.7	20(0.5%)	15.9	415(9.4%)	18	204(4.6%)
25562	Jun 2004	18	350(7.7%)	18	350(7.7%)	19.5	198(4.4%)

26021	Aug 1948	N/A	N/A	14.4	6237(25.6%)	13.9	7116(29.2%)
26091	Jan 2001	24.7	5(0.1%)	16.5	287(7%)	12.9	1002(24.5%)
26095	Jul 2004	19	333(7.3%)	17	633(13.8%)	21.1	172(3.7%)
26099	Jun 2007	26.2	7(0.2%)	13.9	864(26.5%)	17	324(9.9%)
26100	Sep 2003	22.6	14(0.3%)	12.3	1400(28.8%)	15.9	338(6.9%)
26105	Feb 2004	18	304(6.5%)	17	446(9.5%)	18.5	254(5.4%)

Table 1 – Sites used in study with start dates and daily maximum gust speeds for the 28th, 29th and 30th September 2016. All time gust ranking is displayed for each site together with a percentage (in brackets), which refers to the strength of the gust shown as a percentage of the site's full record. Site numbers determined by the BoM, based on state and district (see http://www.bom.gov.au/climate/cdo/about/site-num.shtml#tabulated).

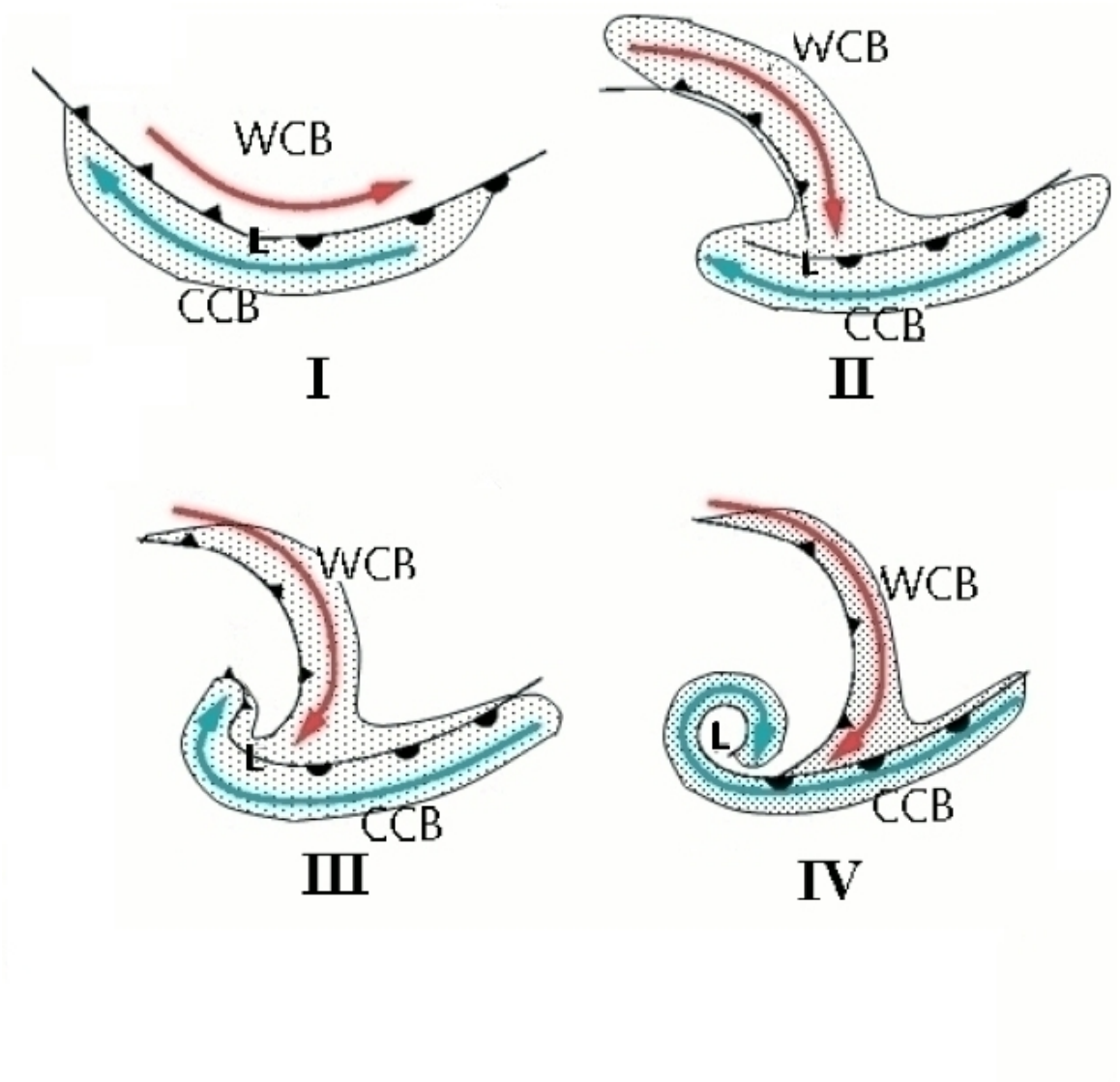

Figure 1. Shapiro-Keyser conceptual model of the life cycle of an extra-tropical cyclone: (I) open wave, (II) frontal fracture, (III) bent-back front and frontal T-bone, and (IV) mature, frontal seclusion (adapted for the southern hemisphere). The cold and warm conveyor belts (CCB and WCB respectively) are marked along with the low pressure centre (L) and the cloud signature (stippled areas) (adapted from Baker 2009).

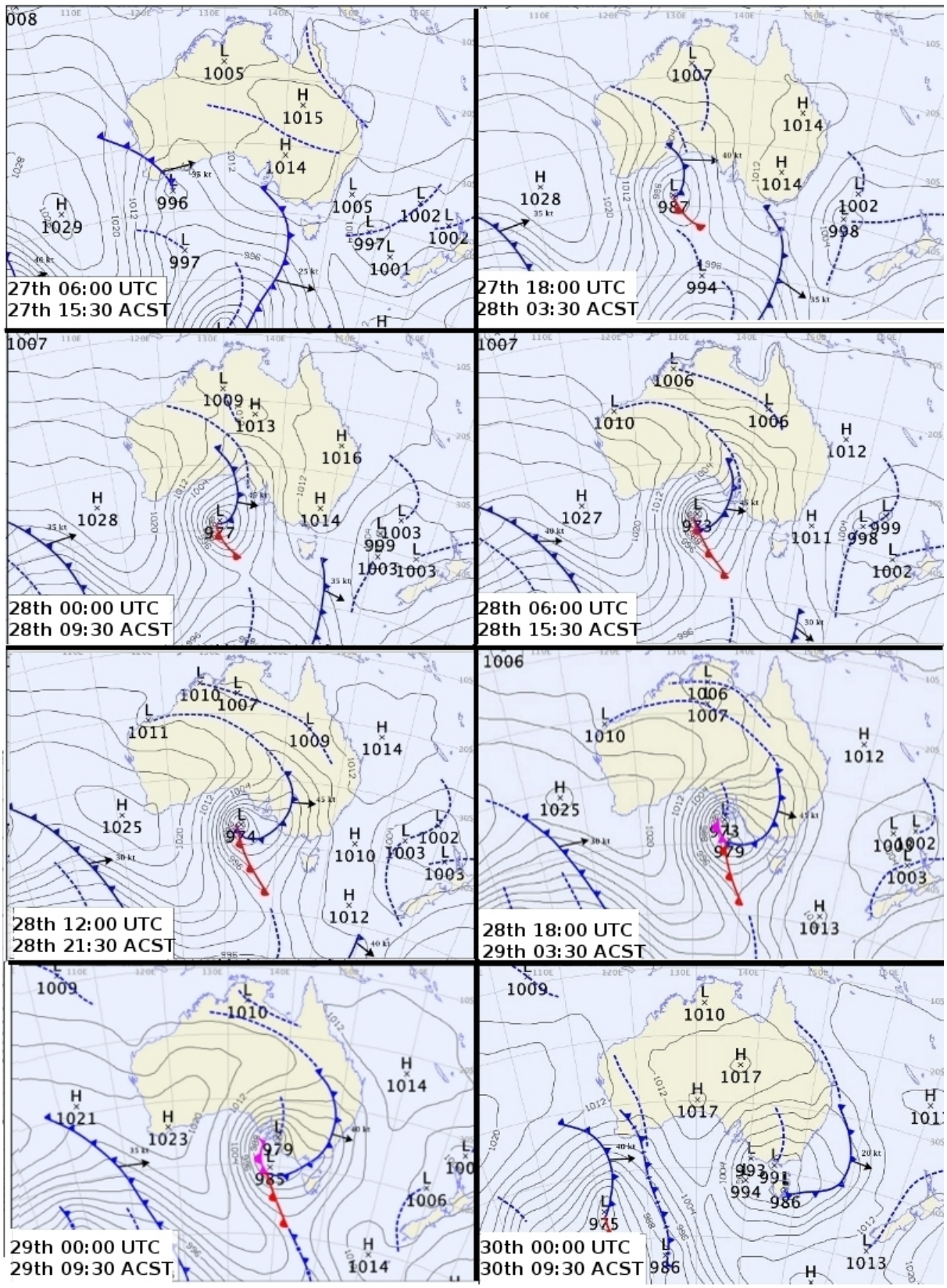

Figure 2 – Selection of synoptic charts to highlight the ETC development from the 28th – 30th September (courtesy of the BoM)

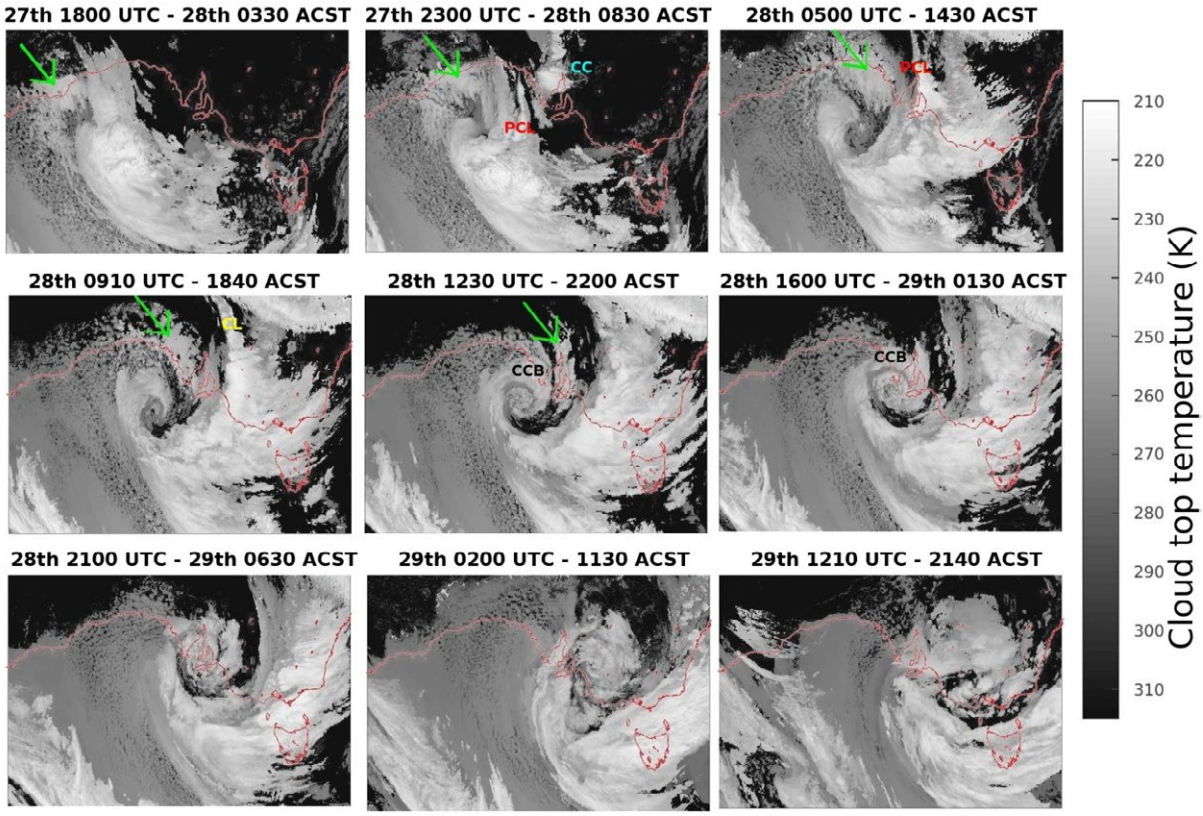

Figure 3 – Cloud top temperatures from Himawari during ETC28. Times in UTC and ACST (UTC + 9:30). Green arrow indicates the moist air getting wrapped up in the dry slot. The Cellular Convection, Psuedo-Convective Line, Convective Line and Cold Conveyor Belt are also marked.

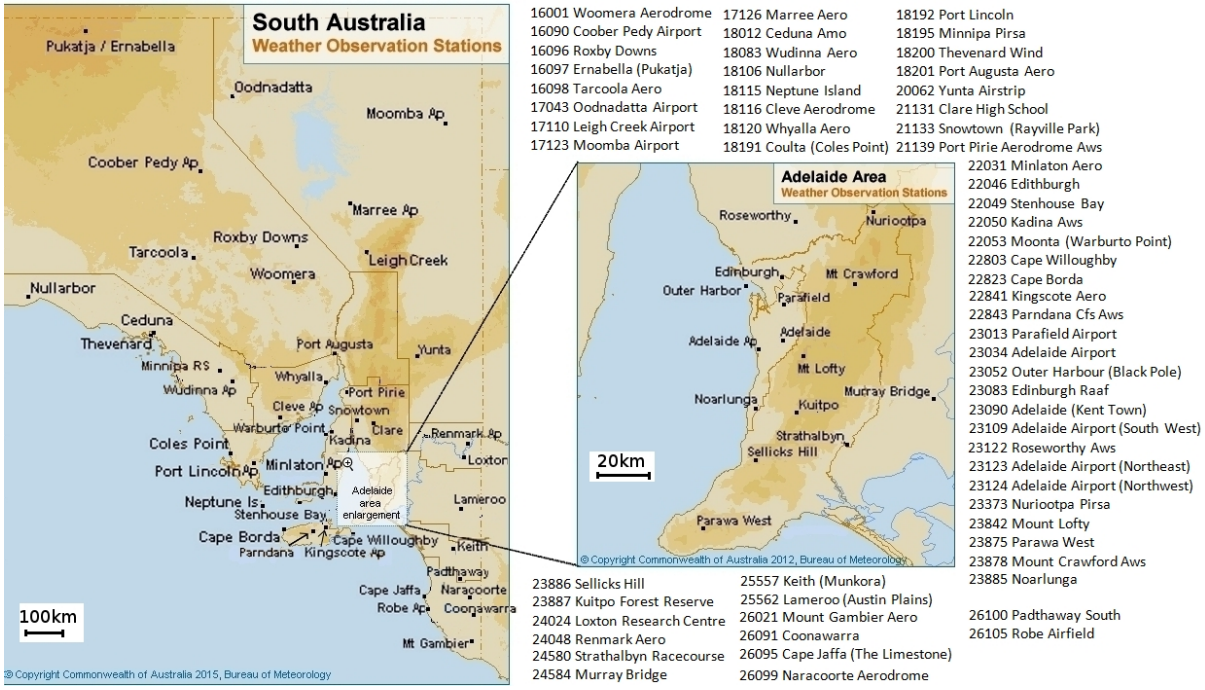

Figure 4 – Site map of South Australia with BoM site numbers.

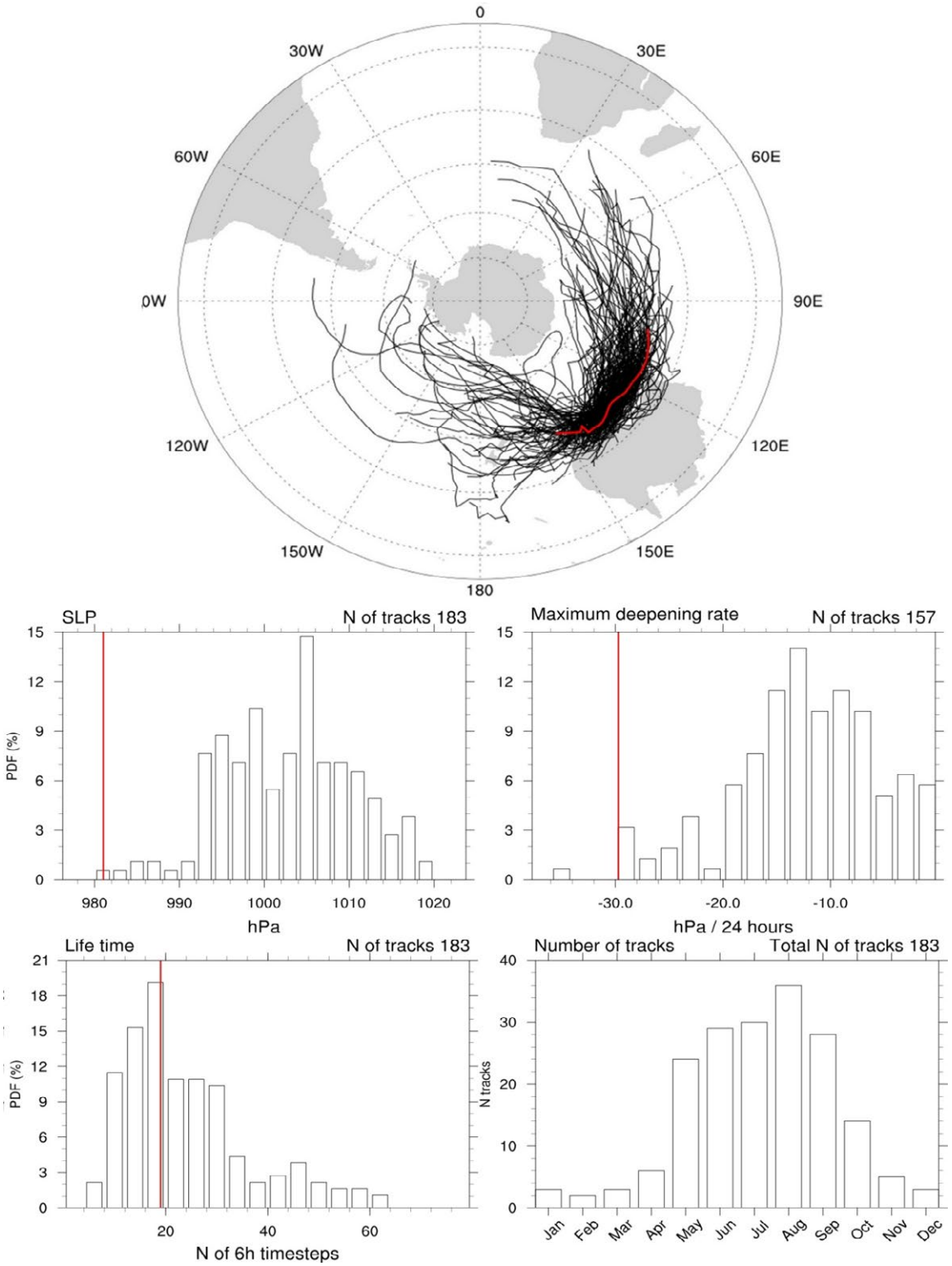

Figure 5. (Top) Tracks of ETCs that were generated over the Southern Indian Ocean and later moved across Adelaide (their centre identified with 5˚ box centered over Adelaide). The red

line shows ETC28. (Top left histogram) ETC central pressures while they move across Adelaide (as above). (Top right histogram) Normalised maximum deepening rate for cyclones shown in the top panel *note that there were 157 tracks, due to 26 ETCs not deepening during the life cycle. (Bottom left histogram) Life time of ETCs. (Bottom right histogram) Number of ETCs affecting Adelaide for each month.

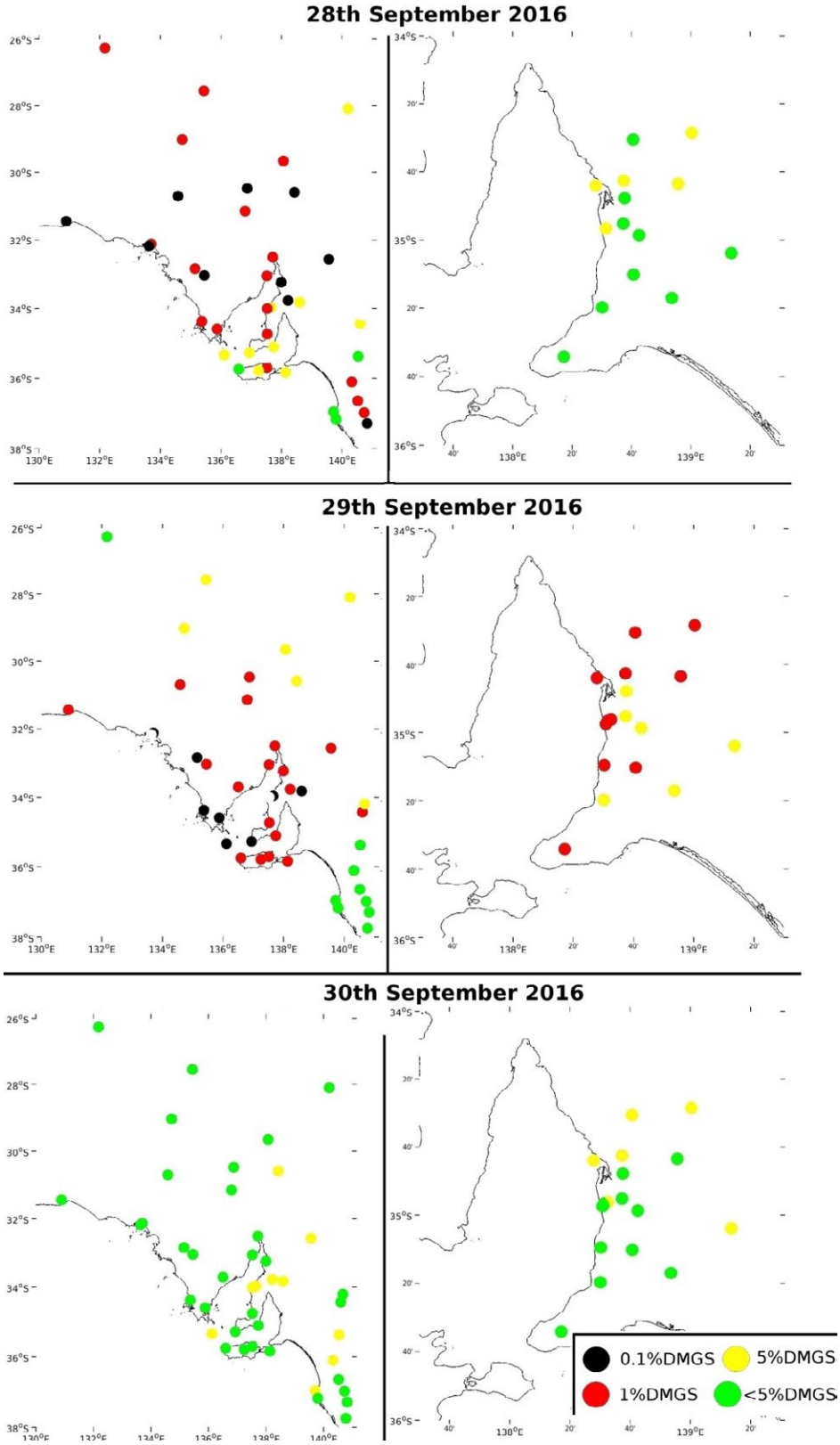

Figure 6. Location of observed surface gusts for the 28th, 29th and 30th September 2016, for top 0.1, 1 and 5 percentiles and below.

Sub-synoptic-scale features associated with extreme surface gusts during the South Australia Storm of September 2016 – Part I: Characteristics of the event

Nick Earl*[1,2], Ian Simmonds[1] and Irina Rudeva[1]

[1] School of Earth Sciences, The University of Melbourne, Parkville, Melbourne, Victoria, 3010, Australia.

[2] Institute for Marine and Antarctic Studies, The University of Tasmania, Hobart, Tasmania, 7003, Australia.

*corresponding author – nearl@unimelb.edu.au

Abstract

Winds are one of the major contributors to deaths, damage and insured losses in Australia. A 'freak storm', which left 1.7 million people without power, hit the state of South Australia on the 28th September 2016, causing state-wide blackouts. In the first part of this two part study, we analyse this event and find that it was indeed extreme, deepening more explosively than all but two Adelaide-affecting extra-tropical cyclones over the past 37 years and exhibiting the lowest central pressure. This generated hurricane force winds, with central South Australia site of Neptune Island recording a gust of over 120kmh^{-1}. We show that this storm potentially contained a sting jet. Such jets are well known to cause major damage over Europe, and this is the first study which investigates whether a sting jet can be produced over Australia. The main deepening of the system occurred over the Great Australian Bight, so if a sting jet did form and make it to the surface, it was not the cause of the state-wide damage. However, the cyclone did contain numerous extreme gust-producing mesoscale features as explored in part II of this paper.

Introduction

Extreme winds are one of the major contributors to deaths, damage and insured losses in many parts of the world. In Australia, these occur on a wide range of spatial scales throughout the continent, yet we poorly understand the diverse and variable causal processes. Systems associated with these winds include fronts, downbursts and tornadoes from supercells or bow echoes, tropical cyclone (TC) and extratropical cyclone (ETC) development. These are more or less dominant in different parts of Australia, with TCs affecting the northern regions and ETCs causing damage and destruction in the south. For example, the wind contributed to the US$1 billion loss from TC Oswald of 2013 and the US$0.9 billion loss from the Brisbane storm of November 2014 (Swiss Re 2017). As to ETCs a notable example of these occurred off New South Wales in June 2007. It caused severe wind and rain damage, resulting in 10 deaths, and insurance claims of around US$1.3 billion, making it one of the most costly natural disasters in Australia's history (Mills *et al. 20*10). ETCs differ from TCs in that they are driven by the contrast in temperatures in the mid-latitudes, and hence only affect the southern states and also possess many different features which cause surface gusts. These include frontal systems, which move from west to east along the Southern Ocean polar front and East Coast Lows which develop off the east coast of New South Wales and Victoria, driven by a complex combination of baroclinicity and conducive atmospheric background conditions (Chambers *et al*. 2014, 2015). Polar front ETCs commonly affect the southern states of Australia during winter, but not so much during summer. These storm tracks have been found to be shifting southwards in the warming climate (Frederiksen and Frederiksen 2007; Pezza *et al. 20*07; Rudeva and Simmonds 2015) However they still produce damaging winds when they affect Australia.

On the 28th September, an extreme ETC (hereafter ETC28) impacted the state of South Australia causing state-wide blackouts and damage. The Australian Bureau of Meteorology (BoM) describes the synoptic scale development of ETC28 from the time of affecting south-west Western Australia on the 27th (BoM 2016). For similar ETC events over the UK, Earl *et al.* (2017) highlighted the many mesoscale features which produce extreme surface winds varying greatly in gust severity, frequency, swath and position relative to the low pressure centre. We provide comprehensive analysis of ETC28 in a two-part paper. Here, we ascertain the extent to which the ETC track and its development were unusual and also put the ETC into longer term context by analysing the gusts compared to previous events detected by the surface station network. We also determine whether ETC28 is a candidate for containing a sting jet (Browning 2004), by analysing the ETC's development. Wind direction is also very important with regard to insured losses (Khanduri and Morrow 2003). Anecdotal reports suggest, for example, an ETC event in February 2005 was especially damaging (relative to the wind speeds observed) in Melbourne and northern Tasmania because the winds were easterly, a rare direction for strong winds in the region. This paper includes wind direction in feature identification and can also give insights into potential damage. In part II we highlight which aspects of the ETC caused the most severe surface wind gusts, and to establish whether Australian ETCs exhibit similar behaviours to their western Europe counterparts. This is the first southern hemisphere ETC to be split into different sub-synoptic scale features in this way, with its extremity based on surface wind observations.

Extra-tropical cyclones

Research into the structure of ETCs has a rich history, since the development of the first conceptualised ETC life-cycle model, the Norwegian cyclone model, developed at the Bergen Geophysical Institute in the late 1910s. It located cyclogenesis along the Northern Hemisphere polar front and dividing the cycle into stages of the typical life of a low pressure system in the extra-tropics (e.g. Parton *et al. 20*10). This formed the basis for the conveyor belt paradigm of Browning (1971) and the development of the Shapiro and Keyser (1990) cyclone model (Figure 1). Not all explosively deepening ETCs follow the Shapiro-Keyser conceptual model life cycle. It is dependent on whether the ETC is embedded in diffluent or confluent large-scale flow in the upper-levels, with the former producing ETCs more likely to follow the Norwegian life-cycle model (see Schultz *et al., 1*998). Schultz and Vaughan (2011) provided a modified view of the occlusion front paradigm within the Norwegian cyclone model suggesting that the occlusion process is the ETC as wrapping-up (differential rotation further from the ETC centre) rather than the cold front catching-up the warm front. Their approach resolved anomalies within the conceptual model and provides a better and more general fluid-dynamical description of the occlusion process.

Sting jet

During the passage of ETCs over western European, Browning (2004) highlighted that the most extreme surface winds were due to a mesoscale feature at the tip of the cloud head known as a sting jet (SJ). These are a short lived (a few hours), mesoscale features associated with strong evaporation at the tip of the cloud head hook, enhancing the dry slot

windspeeds, dubbed the 'sting in the tail' (Browning 2004; Clark et al. 2005). Latent heat used during the evaporation of cloud droplets and rainfall within this region of slantwise descent results in strong gusts that can reach the surface, though some researchers have described cases in which moist processes were not important (e.g. Schultz and Sienkiewicz 2013; Baker et al 2014; Smart and Browning 2014; Slater et al. 2015). Conditional symmetric instability (Gray et al. 2011) in, and upwind of, the dry slot region can produce mesoscale slantwise circulations, also contributing to the severity of the SJ. This was proven to be the case for the UK '16th October 1987 Storm' (Clark *et al. 20*05), ETC Jeanette in October 2002 (Parton *et al. 20*09), ETC Christian in October 2013 (Browning *et al. 20*15) and others. Martínez-Alvarado *et al.* (2012) suggested that SJs are a generic feature of ETCs occurring in between 23 and 32% of the strongest ETCs affecting western Europe. Furthermore, recent work by Martínez-Alvarado et al (2018) found that the proportion of ETCs with a proven SJ precursor (midtropospheric atmospheric instability to slantwise descent diagnosed using downdraught slantwise convective available potential energy) increases to 45% in a future warmer climate. There is no study in the literature that examines whether SJs occur over the Australian continent, despite the southern part of this region experiencing European-like ETCs especially during winter and could become more influential in the future.

28th-30th September 2016 South Australia ETC

ETC28 was one of the most significant Australian ETC events in recent decades. Despite the BoM surface pressure charts resembling the Norwegian model (Figure 2), our analysis concludes that it closely followed the Shapiro-Keyser model, with a bent back cloud head and frontal fracture visible in the satellite images (Figure 3). The Shapiro-Keyser model was

developed for eastern Atlantic Ocean and western European ETCs, but apply broadly to marine extratropical cyclones in the Australian region (Sinclair and Revell 2000), with a bent back cloud head and frontal fracture from the low-pressure-centre as it developed. The 28th saw damaging winds, leading to a South Australia-wide blackout. A total of 23 pylons on electricity transmission lines were damaged, including three of the four interconnectors connecting the Adelaide area to the north and west of the state, leading to cascading failure of the electricity transmission network.

Early on the 27th, an upper level trough became 'cut off' from the polar jet as it travelled east, entering South Australia. This resulted in a transfer of vorticity to the surface, driving explosive deepening of ETC28 in the Great Australian Bight. The synoptic charts (Figure 2) and satellite images (Figure 3) suggests frontal fracture occurring around 0000 UTC on the 28th and the bent back cloud head clearly visible at 0500 UTC. The central pressure fell 23 hPa (according to the BoM) in 24 hours from 0600 UTC on the 27th to 0600 to be 973 hPa on the 28th as highlighted in Figure 2. Once corrected to 60° latitude (sin Φ/sin60), this deepening of over 1 Bergeron is considered a ‘bomb’ in the terminology of Sanders and Gyakum (1980). Lim and Simmonds (2002) have generalised this criterion to take into account the change in climatological mean sea level pressure (SLP) as the cyclone moves into different regions. This is known to be an important factor in the southern hemisphere which is characterised by strong meridional gradients of SLP. However, the motion of ETC28 was predominantly zonal, and the storm still qualified as an ‘explosive developer’ even with this more restrictive definition.

The explosive development occurred in the Great Australian Bight and the ETC centre did not reach landfall until well into stage IV of its life cycle around 0000 UTC on the 29th. 'Supercell thunderstorms' formed along the cold front causing the destructive winds, with 'at least seven tornadoes', hail and very intense rain on the 28th (BoM 2016). Much research, as reviewed by Schenkman and Xue (2016), has focused on mesovorcites and tornadoes forming along convective lines (explored in part II), so this is likely to be the case for ETC28. These affected a vast swath of South Australia and caused considerable damage, including widespread power outages. The preceding months were very wet in South Australia and this moisture excess was enhanced by precipitation along a trough in front of the cold front a few hours prior to the cold front. Clear skies led to strong surface heating after this precipitation, which had raised the dew point temperatures and convective available potential energy, all contributing to this development along the cold front, together with the temperature contrast behind the front. Our analysis explores how the large scale pattern set itself in the days prior to the event, and does this, in part, by using a cyclone-tracking algorithm to determine the origin and evolution of the storm.

Data and methods

Data

Reanalysis data utilised in this study are from the European Centre for Medium-Range Weather Forecasts Reanalysis (ERA)-Interim (Dee *et al. 20*11) project at 6-hour and 0.5˚ latitude-longitude resolution (1979-2016). Surface wind gust speed and direction observations are taken from the BoM website (datasets ranging from 1939-present to 2015-

present (see Table 1)). BoM 6 hourly synoptic charts and 10 minute radar precipitation rate images are also used. Satellite imagery is from the geostationary Himawari platform at 10 minute temporal resolution. These high temporal resolution datasets (especially the radar, available here http://www.theweatherchaser.com/radar-loop/IDR643-adelaide-buckland-park/2016-09-28-04/2016-09-29-04) are crucial, allowing us to observe the exact location of the ETC features, from their precipitation signals.

Methods

ETC tracks are identified using the scheme developed at the University of Melbourne and described in Simmonds and Keay (2002) and Keable *et al.* (2002). The algorithm objectively identifies and tracks cyclones at 6-hourly intervals based on the structure of SLP fields derived from the ERA-Interim reanalysis. This scheme has been used in a range of analyses of cyclone activity in both hemispheres and its results are in good agreement with other methods used for cyclone identification and tracking (e.g. Pinto *et al. 20*05; Raible *et al. 20*08; Simmonds *et al. 20*08; Neu *et al. 20*13).

The daily maximum gust speeds (DMGSs) are ranked in order of intensity for each of the 61 BoM operational observational network sites (Figure 4) for all available data. With the wide-range of site operational lifetimes, we highlight the length of record at each site in Table 1 and when mentioned in the text. DMGSs reaching the top 5%, 1% and 0.1% (hereafter, 5DMGS, 1DMGS and 0.1DMGS; based on number of data points rather than lifetime because of data dropouts) during the 28th, 29th and 30th September 2016 are highlighted at

each site (following the method of Earl *et al.* (2017)). During the development of a windstorm loss model, Hewston (2008) highlighted that it was the top 2% of local DMGSs at specific locations, rather than the absolute wind speeds themselves, that resulted in most damage to UK insured property. Concentrating here mainly on the 1DMGSs and 0.1DMGSs therefore places specific emphasis on the most damaging and life-threatening winds, with the 5DMGSs providing additional information.

Results and discussion

Storm track

Track analysis highlights that ETC28 formed over the southern Indian Ocean on the 26th September and reached South Australia two days later (Figure 2). To put this into a climatological perspective we analysed all ETCs (1979-2016) that had similar trajectories, namely generated over the South Indian Ocean (east of 120^{o}E and south of 35^{o}S) and then moved across a 5˚x 5˚ (136.5-141.5^{o}E, 32.5-37.5^{o}S) box centred over Adelaide. Some ETCs reach Adelaide from the continent (not shown), however, we are only interested in ETCs that have a similar track to ETC28. We found 182 other ETCs that followed a similar trajectory, and tend to occur during the cooler months including September (Figure 5).

Of the 183 tracks, ETC28 had the lowest SLP in the cyclone centre when it moved across Adelaide (Figure 5). Our tracking analysis shows that It possessed the third fastest 24-hour deepening, 21.2hPa and, after latitude normalization (Sanders and Gyakum, 1980), is rated as an ‘explosive developer’ (1.24 Bergeron). This shows that ETC28 was an extreme ETC for this area, a one in ten year event, with comparable ETCs usually tracking further south (Lim

and Simmonds 2002). In the following two sub-sections we explore the surface wind association with this intense ETC, and determine where and why the strongest gusts occurred.

Strongest gust locations

Figure 6 displays the locations of observed surface gusts for each day ETC28 was affecting South Australia (also displayed in Table 1). The 28th and 29th both experienced multiple extreme gusts, whereas by the 30th ETC28 had weakened over South Australia.

28th September

On the 28th, the sites which experienced the strongest winds were spread throughout the state, however the Adelaide Metropolitan area was spared any 1DMGSs. Numerous sites experienced amongst their strongest ever gusts, for example the most western South Australia BoM site, Nullarbor (Figure 4) experienced the 2nd strongest gust (27.8 ms^{-1}; see Table 1 for all gust rankings) in its 28-year history and Leigh Creek (26.2 ms^{-1}), in east South Australia (800km east of Nullarbor), recorded its 6th strongest gust its 34-year history. Of the 55 BoM sites which recorded DMGSs that day (some dropped out perhaps due to the wind), the strongest was 31.4 ms^{-1} at Yunta airstrip and was the strongest gust ever recorded here in its 13 years of recording. The times of the 0.1DMGSs are displayed in Table S1, which highlights the wide ranging times of 0.1DMGSs experienced at each site, for example the gust at Leigh Creek occurred at 20:19 ACST, but Yunta (300km SSE) occurred 2:30hrs earlier at 17:50 ACST. When examined in more detail with satellite/radar and synoptic charts

(Figures 2 and 3), it is clear that the Yunta gust occurred as the cold front moved over the site, however the Leigh Creek site occurred far behind the front (discussed below in part II). It is noteworthy that some sites located near those mentioned above did not produce even a 1 in 20 day (or top 5%) gust. Coastal sites Cape Jaffa (19 ms^{-1}) and Robe Airfield (18 ms^{-1}) DGMSs were outside the 5th percentile, whereas Coonawarra, just 100km inland produced the 5th strongest gust (24.7 ms^{-1}) in its 15-year history. This highlights the fact that wind producing features within storms vary greatly spatially. Also, some sites usually sheltered from the prevailing south-westerly wind are more exposed from other directions. However, DMGSs were mainly northerly the 28th (see Table S1 for gust direction), which is a common wind direction according to the BoM (http://www.bom.gov.au/climate/averages/wind/selection_map.shtml). Therefore, the orientation of the DMGSs were unlikely to have contributed to the widespread damage to transmission lines, leading to the state-wide blackout on the 28th. Many of the damaged transmission lines were in the Port Augusta area (Figure 4; central South Australia, 300 km north of Adelaide), and this site experienced a 1DMGS from the NNE.

2) *29th September*

On the 29th, the low-pressure-centre tracked just south of Adelaide metropolitan area. This brought 1DMGSs to the central part of South Australia, while the far north and southeast were unaffected. The pattern of DMGS percentiles is less sporadic than the previous day, with the grouping together of similar severity of DMGSs. The strongest South Australia DMGS recorded throughout ETC28 occurred on the exposed Neptune Island, 33.4 ms^{-1}, the 4th strongest DMGS seen since recording began in January 1985. The coastal Ceduna site in

western South Australia clocked the 2nd strongest DMGS, 31.9 ms^{-1}, the 10th strongest gust of its 76-year history, with its neighbour, Thevenard not recording, possibly due to damage. Figure 6 shows how many sites experienced 0.1DMGSs and 1DMGSs on the perhaps less infamous 29th September (compared with the 28th) with numerous 1DMGSs affecting the Adelaide metropolitan area. The timing of most 1DMGSs affected the surface sites in the vicinity of the low-pressure-centre as it migrated eastward.

30th September

The ETC was moving off eastward on the 30th with just a handful of 5DMGSs. The severity of DMGSs affecting the Adelaide area was comparable to the 28th. There were no 1DMGSs recorded on the 30th, but Edinburgh RAAF site recorded a top 2% gust which occurred along the occluded front, as the main system past.

Sting jet

Explosive deepening of an ETC is one of the main contributing factors towards the formation of sting jets within them (Browning 2004). The main development occurred offshore and the ETC centre did not make landfall until well into stage IV of its life cycle around 0000 UTC on the 29th. This means that it is very unlikely that any extreme winds experienced during ETC28 were caused by a SJ (only seen in stages II and III of the Shapiro-Keyser life cycle model) and that other mechanisms were responsible for the extreme surface winds as explored in part II. If a SJ did form and reach the surface, this is likely to have occurred in the Great Australian Bight but certainly did not make landfall. However, as mentioned, ETC28

deepened explosively and had a clear bent back cloud head with likely evaporation at the tip of the cloud head hook, seen on the 28th (Figure 3). As SJs are likely to be a generic feature of ETCs (Martínez-Alvarado *et al. 20*12), ETC28 looks likely to have contained one. However, the lack of observations makes it impossible to prove without modelling (by following the method of Smart and Browning (2014)), which is outside the scope of this paper. With SJs predicted to be more influential in the future (Martínez-Alvarado *et al.* 2018) the study of Australian SJ is imperative.

Conclusions

ETCs commonly affect southern Australia and ETC28 was an extreme among these. The storm was one of the most intense storms to hit the state of South Australia in recent decades, and left millions without power and brought the state to a standstill. This region is prone to ETCs and the question was raised as to why this particular ETC was so damaging, described anecdotally as a 1 in 50 year event? What were the specific characteristics that created such severe surface winds? The ETC progressed along a prevalent track and followed the Shapiro-Keyser life cycle model common in European explosive ETCs. However, of these similar-tracking ETCs, the ETC28 low pressure centre deepened more explosively than all but two over the past 37 years and reached the lowest central pressure of all. With this explosive development, ETC28 potentially contained a SJ, however this deepening occurred offshore, so if a SJ made it to the surface, it was not the cause of the state-wide damage. The storm contained numerous extreme gust-producing mesoscale features as explored in part II of this paper.

Acknowledgements

Parts of this research were made possible by funding from the Australian Research Council

(ARC) Grant DP16010997. Nick Earl was also supported by the ARC (CE110001028).

References

Atkins NT, Bouchard CS, Przybylinski RW, Trapp RJ, Schmocker G. 2005. Damaging surface wind mechanisms within the 10 June 2003 Saint Louis bow echo during BAMEX. *Mon. Weather. Rev.*, 133(8): 2275-2296

Baker LH, Gray SL, Clark PA. 2014. Idealised simulations of sting-jet cyclones. *Q. J. R. Meteorol. Soc.* 140: 96–110.

Browning KA. 1971. Radar measurements of air motion near fronts. *Weather*. 26(8): 320-340.

Browning KA. 2004. The sting at the end of the tail: Damaging winds associated with extratropical cyclones. *Q. J. R. Meteorol. Soc.* 130: 375-399. doi: 10.1256/qj.02.143.

Browning KA, Smart DJ, Clark MR, Illingworth AJ. 2015. The role of evaporating showers in the transfer of sting-jet momentum to the surface. *Q. J. R. Meteorol. Soc.* 141: 2956–2971. doi.org/10.1002/qj.2581.

Bureau of Meteorology. 2016. Severe thunderstorm and tornado outbreak South Australia 28 September 2016. 54 pp. http://www.bom.gov.au/announcements/sevwx/sa/Severe_Thunderstorm_and_Tornado_Outbreak_28_September_2016.pdf.

Chambers, C. R. S., Brassington, G. B., Simmonds, I. and Walsh, K. 2014. 'Precipitation changes due to the introduction of eddy-resolved sea surface temperatures into simulations of the "Pasha Bulker" Australian east coast low of June 2007', *Meteorol. Atmos. Phys*., 125, 1-15, doi: 10.1007/s00703-014-0318-4.

Chambers, C. R. S., Brassington, G. B., Walsh, K. and Simmonds, I. 2015. 'Sensitivity of the distribution of thunderstorms to sea surface temperatures in four Australian east coast lows', *Meteorol. Atmos. Phys*., 127, 499-517, doi: 10.1007/s00703-015-0382-4.

Clark PA, Browning KA, Wang C. 2005. The sting at the end of the tail: Model diagnostics of fine-scale three-dimensional structure of the cloud head. *Q. J. R. Meteorol. Soc.* 131(610): 2263-2292.

Dee DP, Uppala SM, Simmons AJ, Berrisford P, Poli P, Kobayashi S, Andrae U, Balmaseda MA, Balsamo G, Bauer P, Bechtold P. 2011. The ERA-Interim reanalysis: Configuration and performance of the data assimilation system. *Q. J. R. Meteorol. Soc.* 137(656): 553-597.

Earl N, Dorling S, Starks M, Finch R. 2017. Subsynoptic-scale features associated with extreme surface gusts in UK extratropical cyclone events. *Geophys. Res. Lett.* 44: 3932–3940. doi:10.1002/2017GL073124.

Frederiksen JS, Frederiksen CS. 2011. Twentieth century winter changes in Southern Hemisphere synoptic weather modes. *Adv. Meteorol.* 353829. doi: 10.1155/2011/353829.

Gray SL, Martínez-Alvarado O, Baker LH, Clark PA. 2011. Conditional symmetric instability in sting-jet storms. *Q. J. R. Meteorol. Soc.* 137(659): 1482-1500.

Hewston R. 2008. Weather, climate and the insurance sector. Ph.D. dissertation, University of East Anglia; 312 pp.

Keable M, Simmonds I, Keay K. 2002. Distribution and temporal variability of 500 hPa cyclone characteristics in the Southern Hemisphere. *Int. J. Climatol.* 22: 131-150.

Khanduri AC, Morrow GC. 2003. Vulnerability of buildings to windstorms and insurance loss estimation. *J. Wind Eng. Ind. Aerod.* 91(4): 455-467.

Lim EP, Simmonds I. 2002. Explosive cyclone development in the Southern Hemisphere and a comparison with Northern Hemisphere events. *Mon. Weather. Rev.* 130: 2188-2209.

Martínez-Alvarado O, Gray SL, Catto JL, Clark PA. 2012. Sting jets in intense winter North-Atlantic windstorms. *Environ. Res. Lett.* 7: 024014.

Martínez-Alvarado O, Gray SL, Hart NC, Clark PA, Hodges K, Roberts MJ. 2018. Increased wind risk from sting-jet windstorms with climate change. *Environ. Res. Lett.* 13: 044002.

Mills GA, Webb R, Davidson NE, Kepert J, Seed A, Abbs D. 2010. The Pasha Bulker east coast low of 8 June 2007. Centre for Australia Weather and Climate Research Tech. Rep. 23, 62 pp. [Available online at http://www.cawcr.gov.au/publications/technicalreports.php.]

Neu U, Akperov MG, Bellenbaum N, Benestad R, Blender R, Caballero R, Cocozza A, Dacre HF, Feng Y, Fraedrich K, Grieger J. 2013. IMILAST: A community effort to intercompare extratropical cyclone detection and tracking algorithms. *Bull. Am. Meteorol. Soc.* 94: 529-547. doi: 10.1175/BAMS-D-11-00154.1

Parton GA, Vaughan G, Norton EG, Browning KA, Clark PA. 2009. Wind profiler observations of a sting jet. *Q. J. R. Meteorol. Soc.* 135(640): 663-680.

Parton G, Dore A, Vaughan G. 2010. A climatology of midtropospheric mesoscale strong wind events as observed by the MST radar, Aberystwyth. *Meteorol. Appl.* 17: 340–354. doi:10.1002/met.203.

Pezza AB, Simmonds I, Renwick JA. 2007. Southern Hemisphere cyclones and anticyclones: Recent trends and links with decadal variability in the Pacific Ocean. *Int. J. Climatol.* 27: 1403-1419. doi: 10.1002/joc.1477.

Pinto JG, Spangehl T, Ulbrich U, Speth P. 2005. Sensitivities of a cyclone detection and tracking algorithm: Individual tracks and climatology. *Meteorol. Z*. 14 : 823–838.

Raible CC, Della-Marta PM, Schwierz C, Wernli H, Blender R. 2008. Northern Hemisphere extra-tropical cyclones: A comparison of detection and tracking methods and different reanalyses. *Mon. Wea . Rev.*136: 880–897.

Rudeva I, Simmonds I. 2015. Variability and trends of global atmospheric frontal activity and links with large-scale modes of variability. *J. Clim.* 28: 3311-3330.

Sanders F, Gyakum JR. 1980. Synoptic-dynamic climatology of the "bomb". *Mon. Weather. Rev.* 108: 1589-1606.

Schenkman AD, Xue M. 2016. Bow-echo mesovortices: A review. *Atmos. Res.* 170: 1-13. doi: 10.1016/j.atmosres.2015.11.003

Schultz DM, Keyser D, Bosart LF. 1998. The effect of largescale flow on low-level frontal structure and evolution in midlatitude cyclones. *Mon. Weather. Rev.* 126: 1767–1791.

Schultz DM, Vaughan G. 2011. Occluded fronts and the occlusion process: A fresh look at conventional wisdom. *Bull. Am. Meteorol. Soc.* 92: 443–466 ES19–ES20.

Schultz DM, Sienkiewicz JM. 2013. Using frontogenesis to identify possible sting jets in extratropical cyclones. *Weather Forecasting.* 28: 603–613.

Shapiro MA, Keyser DA. 1990. Fronts, jet streams, and the tropopause. *Extratropical Cyclones: The Erik Palmén Memorial Volume*, C. W. Newton and E. O. Holopainen, Eds*. Am. Meteorol. Soc.* 167–191.

Simmonds I, Burke C, Keay K. 2008. Arctic climate change as manifest in cyclone behavior. *J. Clim.* 21: 5777-5796. doi: 10.1175/2008JCLI2366.1.

Simmonds I, Keay K. 2002. Surface fluxes of momentum and mechanical energy over the North Pacific and North Atlantic Oceans. *Meteorol. Atmos. Phys.* 80: 1-18. doi: 10.1007/s007030200009.

Sinclair MR, Revell MJ. 2000. Classification and composite diagnosis of extratropical cyclogenesis events in the southwest Pacific. *Mon. Weather. Rev.* 128(4): 1089-1105.

Slater TP, Schultz DM, Vaughan G. 2015. Acceleration of near-surface strong winds in a dry, idealized extratropical cyclone. *Q. J. R. Meteorol. Soc.* 141: 1004–1016. doi:10.1002/qj.2417

Smart DJ, Browning KA. 2014. Attribution of strong winds to a cold conveyor belt and sting jet. *Q. J. R. Meteorol. Soc.* 140: 595–610

BoM Site number	Start date	Gust speed 28th (ms^{-1})	Gust rank 28th (top%)	Gust speed 29th (ms^{-1})	Gust rank 29th	Gust speed 30th (ms^{-1})	Gust rank 30th
16001	May 1949	26.7	98(0.5%)	25.2	144(0.7%)	17	2365(11.3%)
16090	Mar 2004	24.2	37(0.8%)	23.1	54(1.2%)	15.4	895(19.1%)
16096	Mar 2007	25.7	4(0.1%)	21.1	25(0.7%)	13.9	650(18.5%)
16097	May 2003	22.1	28(0.6%)	17	272(5.7%)	10.8	2467(51.8%)
16098	Aug 1999	25.7	5(0.1%)	23.7	17(0.3%)	13.4	1279(25.4%)
17043	Mar 1941	25.2	157(0.8%)	19.5	1019(4.9%)	13.9	5261(25.4%)
17110	May 1982	26.2	6(0.1%)	20.6	80(1.6%)	20.6	80(1.6%)
17123	Apr 2005	19.5	57(1.4%)	18	124(2.9%)	12.9	1019(24.1%)
17126	Apr 2003	24.2	40(0.8%)	23.1	53(1.1%)	13.4	1476(30.5%)
18012	Mar 1940	24.7	191(0.7%)	31.9	10(0%)	15.9	5200(19%)
18083	Aug 2003	27.3	6(0.1%)	22.1	47(1%)	14.9	826(17.2%)
18106	Jan 1988	27.8	2(0.1%)	22.1	42(1%)	9.3	3439(85.7%)
18115	Jan 1985	26.7	127(2.7%)	33.4	4(0.1%)	25.2	193(4%)
18116	Jul 2003	N/A	N/A	24.7	26(0.5%)	13.9	1406(29.2%)
18120	Sep 2003	24.2	13(0.3%)	22.6	37(0.8%)	14.9	976(20.4%)
18191	Aug 2003	27.8	7(0.2%)	29.3	3(0.1%)	18	254(5.6%)
18192	Aug 2003	26.7	10(0.2%)	29.8	4(0.1%)	15.4	790(16.6%)
18195	Aug 2003	23.1	15(0.3%)	24.7	5(0.1%)	11.3	2365(49.5%)
18200	Mar 2015	27.8	1(0.1%)	N/A	N/A	18.5	51(7.1%)
18201	Aug 2003	24.7	16(0.4%)	26.2	10(0.2%)	17	379(9.4%)
20062	Jun 2003	31.4	1(0%)	24.2	28(0.6%)	18.5	223(4.6%)
21131	Jul 2003	16.5	174(3.6%)	22.1	5(0.1%)	17.5	100(2%)
21133	Oct 2003	28.8	3(0.1%)	25.2	17(0.4%)	21.1	111(2.3%)
21139	Jan 2015	26.7	1(0.1%)	24.2	5(0.7%)	18	38(5.1%)
22031	Aug 2003	25.2	26(0.5%)	26.7	12(0.2%)	19	306(6.2%)
22046	Jul 1984	20.6	145(2.9%)	23.7	48(1%)	15.4	750(15.2%)
22049	Jul 2003	22.6	85(1.7%)	28.3	2(0%)	17	631(12.8%)
22050	Jul 2005	22.6	47(1.1%)	28.8	1(0%)	20.6	110(2.6%)
22053	Jul 2003	24.2	20(0.9%)	N/A	N/A	21.6	64(2.8%)
22803	Jun 2000	27.3	69(1.6%)	28.3	42(1%)	20.6	538(12.7%)
22823	Feb 2004	20.1	277(6.1%)	27.8	9(0.2%)	17	667(14.7%)
22841	Oct 2003	21.6	48(1%)	23.1	19(0.4%)	16.5	398(8.3%)

22843	Sep 2011	22.6	22(1.1%)	24.7	8(0.4%)	15.9	221(11.1%)
23013	Jul 1939	19	1000(6.2%)	21.6	440(2.7%)	18.5	1208(7.5%)
23034	Feb 1955	21.1	581(2.6%)	23.1	317(1.4%)	17	2135(9.5%)
23052	Mar 2015	23.7	8(1.1%)	26.7	2(0.3%)	22.1	15(2.1%)
23083	Jan 1973	20.6	381(2.9%)	24.7	81(0.6%)	22.1	208(1.6%)
23090	Feb 1977	13.9	1991(13.8%)	19	239(1.7%)	13.9	1991(13.8%)
23109	Oct 2011	N/A	N/A	23.1	7(0.4%)	14.9	166(8.4%)
23122	Aug 1997	17.5	335(6.6%)	24.2	17(0.3%)	19.5	154(3%)
23123	Oct 2011	N/A	N/A	22.6	5(0.3%)	17.5	59(3.1%)
23124	Sep 2011	19	47(2.4%)	22.6	12(0.6%)	16.5	130(6.6%)
23373	Jul 2004	18.5	163(3.6%)	23.1	13(0.3%)	19.5	102(2.3%)
23842	Sep 2004	17.5	380(8.8%)	22.1	60(1.4%)	13.9	942(21.9%)
23875	Jul 2004	17	328(7.2%)	22.6	28(0.6%)	13.9	966(21.2%)
23878	Jun 2004	25.2	51(1.1%)	27.3	18(0.4%)	20.6	256(5.6%)
23885	Apr 2004	N/A	N/A	21.1	46(1%)	14.9	731(15.6%)
23886	Sep 2011	19	108(5.4%)	20.1	65(3.3%)	12.3	851(42.9%)
23887	Aug 2003	17	426(8.7%)	23.1	33(0.7%)	17	426(8.7%)
24024	Nov 1998	17.5	152(2.3%)	19.5	56(0.9%)	14.9	448(6.9%)
24048	Dec 2003	N/A	N/A	20.6	80(1.7%)	17	309(6.5%)
24580	Mar 2004	18.5	287(6.1%)	20.1	165(3.5%)	17.5	390(8.2%)
24584	Mar 2006	17.5	267(6.8%)	19	142(3.6%)	18.5	183(4.7%)
25557	Sep 2004	23.7	20(0.5%)	15.9	415(9.4%)	18	204(4.6%)
25562	Jun 2004	18	350(7.7%)	18	350(7.7%)	19.5	198(4.4%)
26021	Aug 1948	N/A	N/A	14.4	6237(25.6%)	13.9	7116(29.2%)
26091	Jan 2001	24.7	5(0.1%)	16.5	287(7%)	12.9	1002(24.5%)
26095	Jul 2004	19	333(7.3%)	17	633(13.8%)	21.1	172(3.7%)
26099	Jun 2007	26.2	7(0.2%)	13.9	864(26.5%)	17	324(9.9%)
26100	Sep 2003	22.6	14(0.3%)	12.3	1400(28.8%)	15.9	338(6.9%)
26105	Feb 2004	18	304(6.5%)	17	446(9.5%)	18.5	254(5.4%)

Table 1 – Sites used in study with start dates and daily maximum gust speeds for the 28th, 29th and 30th September 2016. All time gust ranking is displayed for each site together with a percentage (in brackets), which refers to the strength of the gust shown as a percentage of the site's full record. Site numbers determined by the BoM, based on state and district (see http://www.bom.gov.au/climate/cdo/about/site-num.shtml#tabulated).

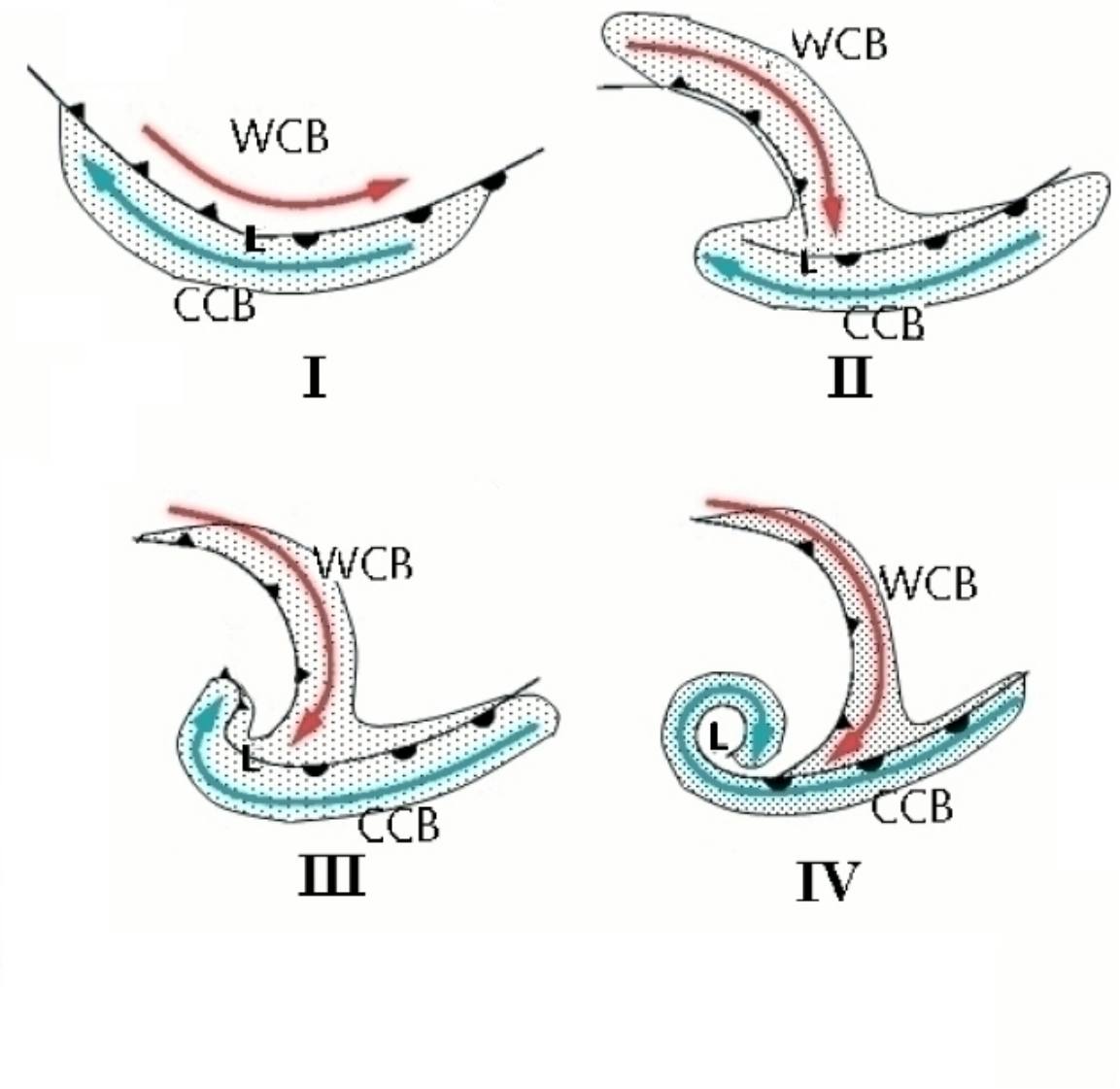

Figure 1. Shapiro-Keyser conceptual model of the life cycle of an extra-tropical cyclone: (I) open wave, (II) frontal fracture, (III) bent-back front and frontal T-bone, and (IV) mature, frontal seclusion (adapted for the southern hemisphere). The cold and warm conveyor belts (CCB and WCB respectively) are marked along with the low pressure centre (L) and the cloud signature (stippled areas) (adapted from Baker 2009).

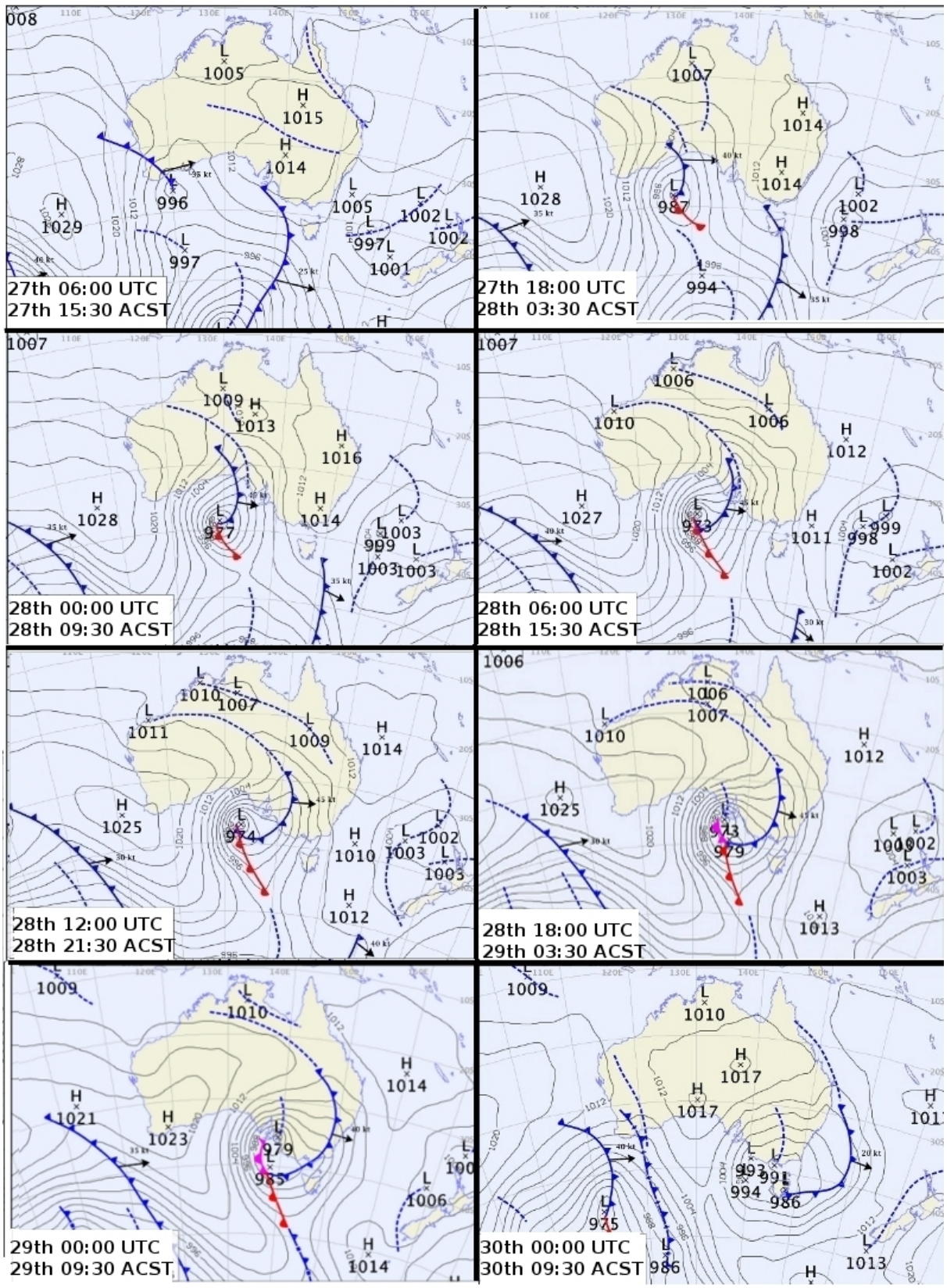

Figure 2 – Selection of synoptic charts to highlight the ETC development from the 28th – 30th September (courtesy of the BoM)

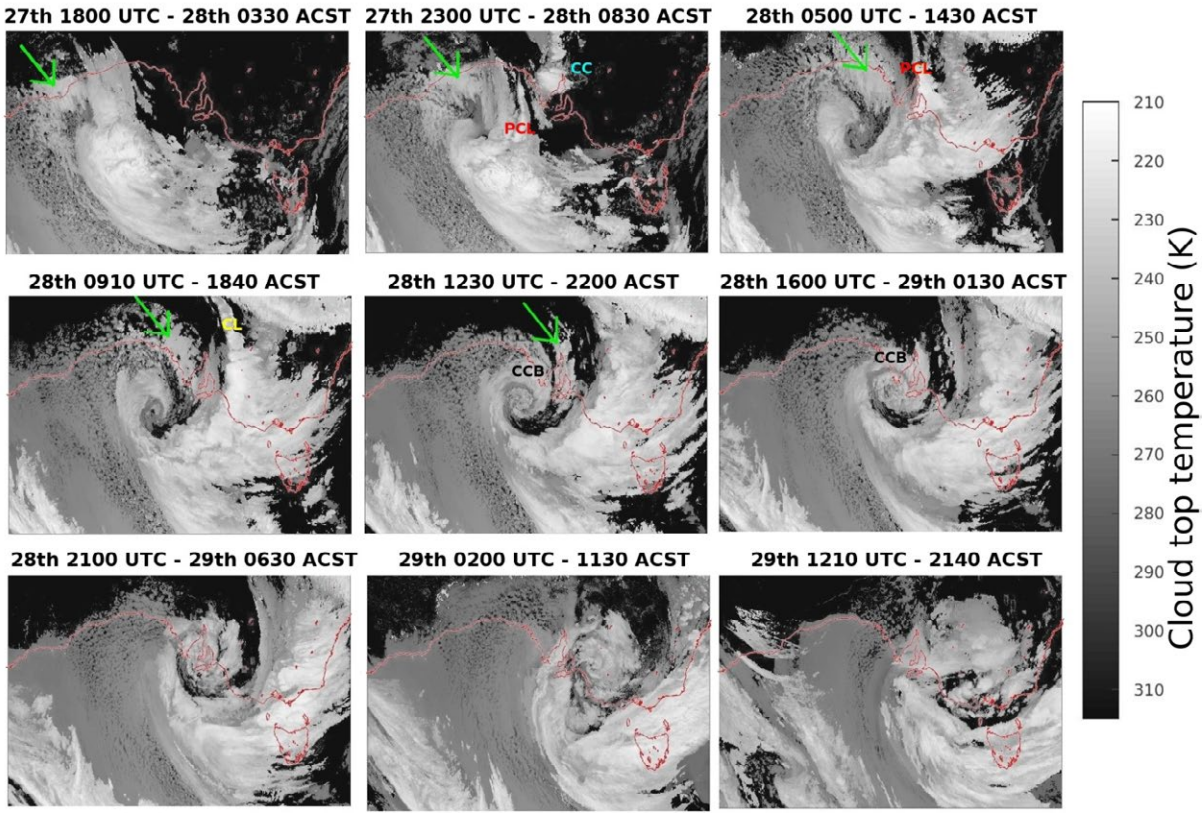

Figure 3 – Cloud top temperatures from Himawari during ETC28. Times in UTC and ACST (UTC + 9:30). Green arrow indicates the moist air getting wrapped up in the dry slot. The Cellular Convection, Psuedo-Convective Line, Convective Line and Cold Conveyor Belt are also marked.

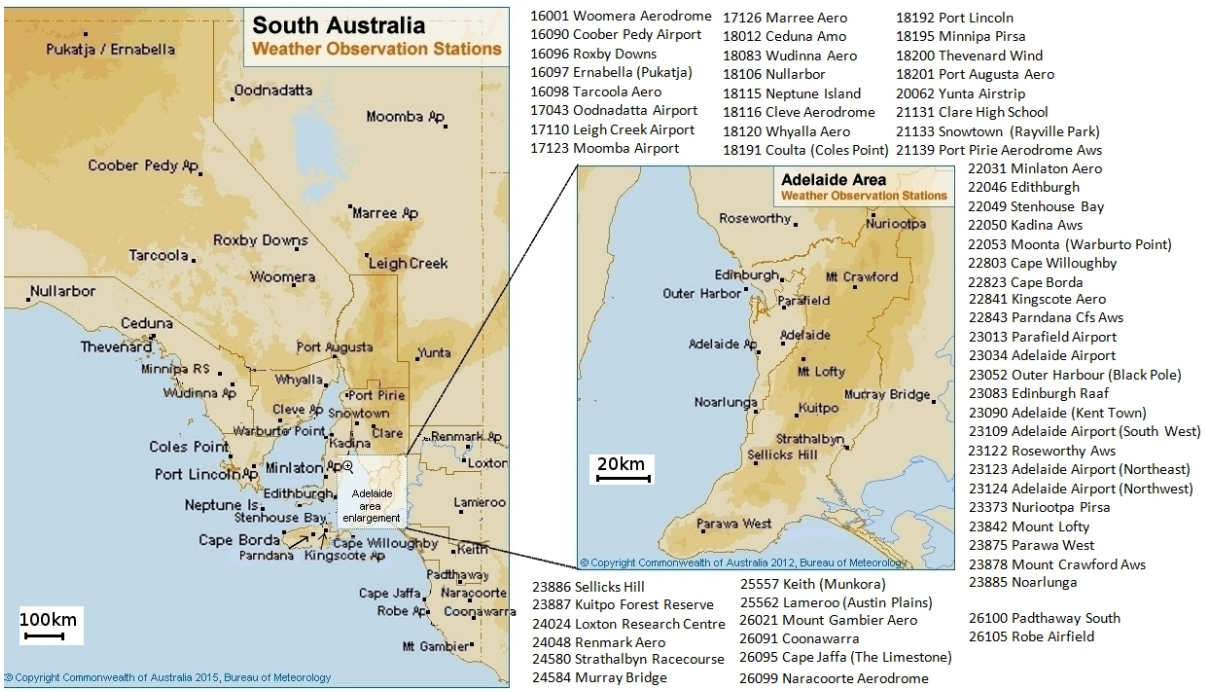

16001 Woomera Aerodrome
16090 Coober Pedy Airport
16096 Roxby Downs
16097 Ernabella (Pukatja)
16098 Tarcoola Aero
17043 Oodnadatta Airport
17110 Leigh Creek Airport
17123 Moomba Airport
17126 Marree Aero
18012 Ceduna Amo
18083 Wudinna Aero
18106 Nullarbor
18115 Neptune Island
18116 Cleve Aerodrome
18120 Whyalla Aero
18191 Coulta (Coles Point)
18192 Port Lincoln
18195 Minnipa Pirsa
18200 Thevenard Wind
18201 Port Augusta Aero
20062 Yunta Airstrip
21131 Clare High School
21133 Snowtown (Rayville Park)
21139 Port Pirie Aerodrome Aws
22031 Minlaton Aero
22046 Edithburgh
22049 Stenhouse Bay
22050 Kadina Aws
22053 Moonta (Warburto Point)
22803 Cape Willoughby
22823 Cape Borda
22841 Kingscote Aero
22843 Parndana Cfs Aws
23013 Parafield Airport
23034 Adelaide Airport
23052 Outer Harbour (Black Pole)
23083 Edinburgh Raaf
23090 Adelaide (Kent Town)
23109 Adelaide Airport (South West)
23122 Roseworthy Aws
23123 Adelaide Airport (Northeast)
23124 Adelaide Airport (Northwest)
23373 Nuriootpa Pirsa
23842 Mount Lofty
23875 Parawa West
23878 Mount Crawford Aws
23885 Noarlunga
26100 Padthaway South
26105 Robe Airfield
23886 Sellicks Hill
23887 Kuitpo Forest Reserve
24024 Loxton Research Centre
24048 Renmark Aero
24580 Strathalbyn Racecourse
24584 Murray Bridge
25557 Keith (Munkora)
25562 Lameroo (Austin Plains)
26021 Mount Gambier Aero
26091 Coonawarra
26095 Cape Jaffa (The Limestone)
26099 Naracoorte Aerodrome

Figure 4 – Site map of South Australia with BoM site numbers.

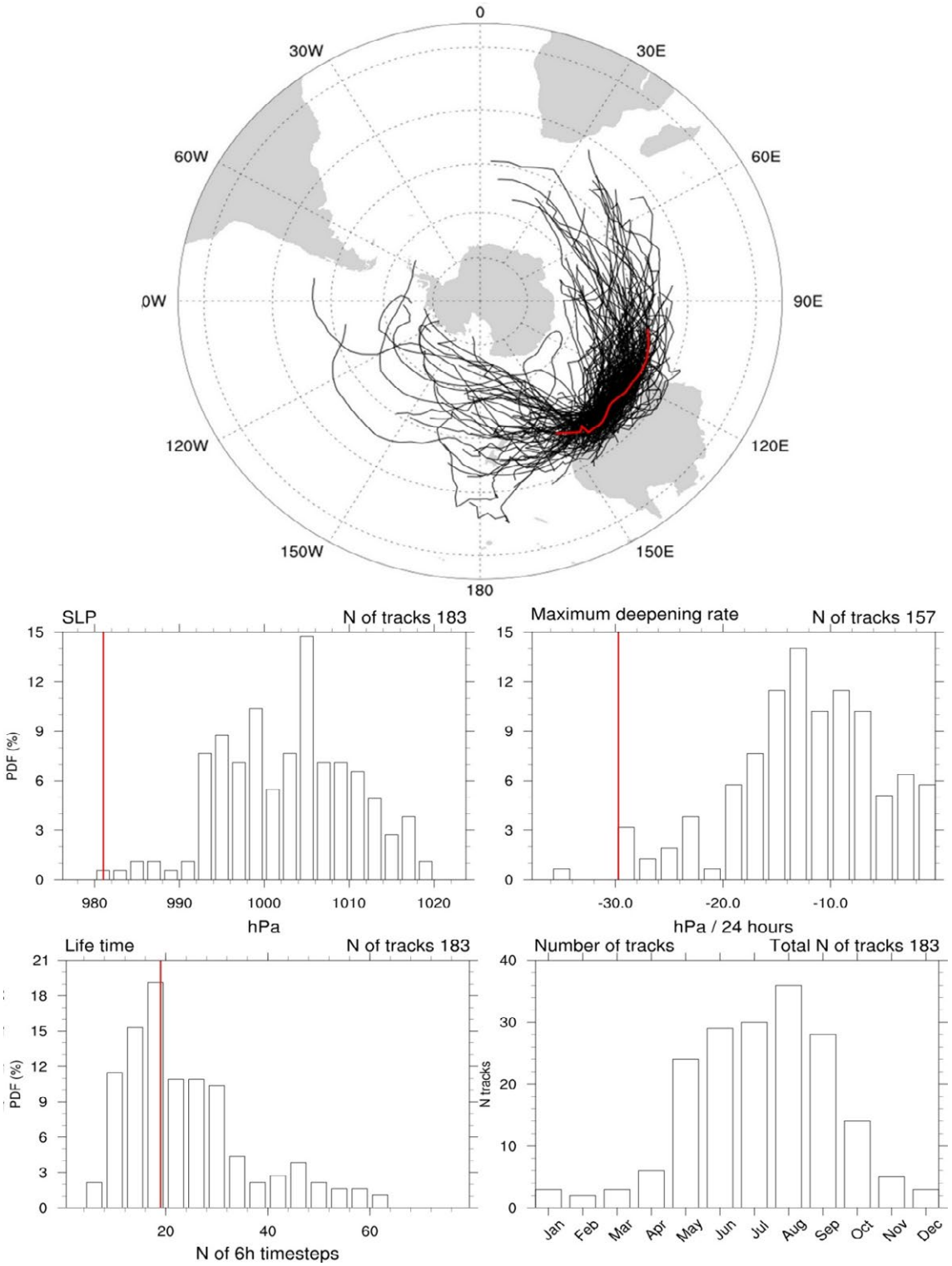

Figure 5. (Top) Tracks of ETCs that were generated over the Southern Indian Ocean and later moved across Adelaide (their centre identified with 5˚ box centered over Adelaide). The red line shows ETC28. (Top left histogram) ETC central pressures while they move across Adelaide (as above). (Top right histogram) Normalised maximum deepening rate for cyclones shown in the top panel *note that there were 157 tracks, due to 26 ETCs not deepening during the life cycle. (Bottom left histogram) Life time of ETCs. (Bottom right histogram) Number of ETCs affecting Adelaide for each month.

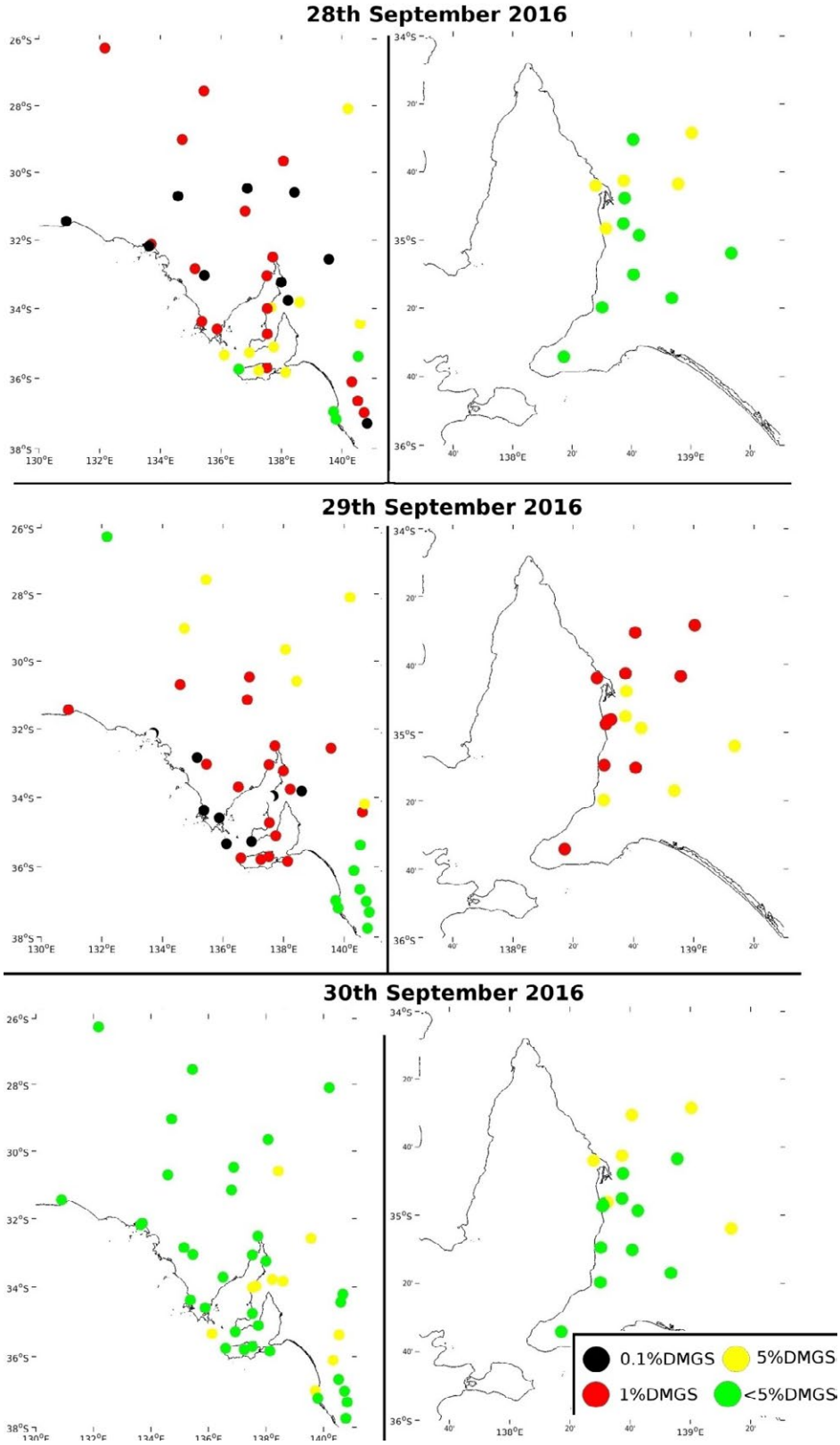

Figure 6. Location of observed surface gusts for the 28th, 29th and 30th September 2016, for top 0.1, 1 and 5 percentiles and below.

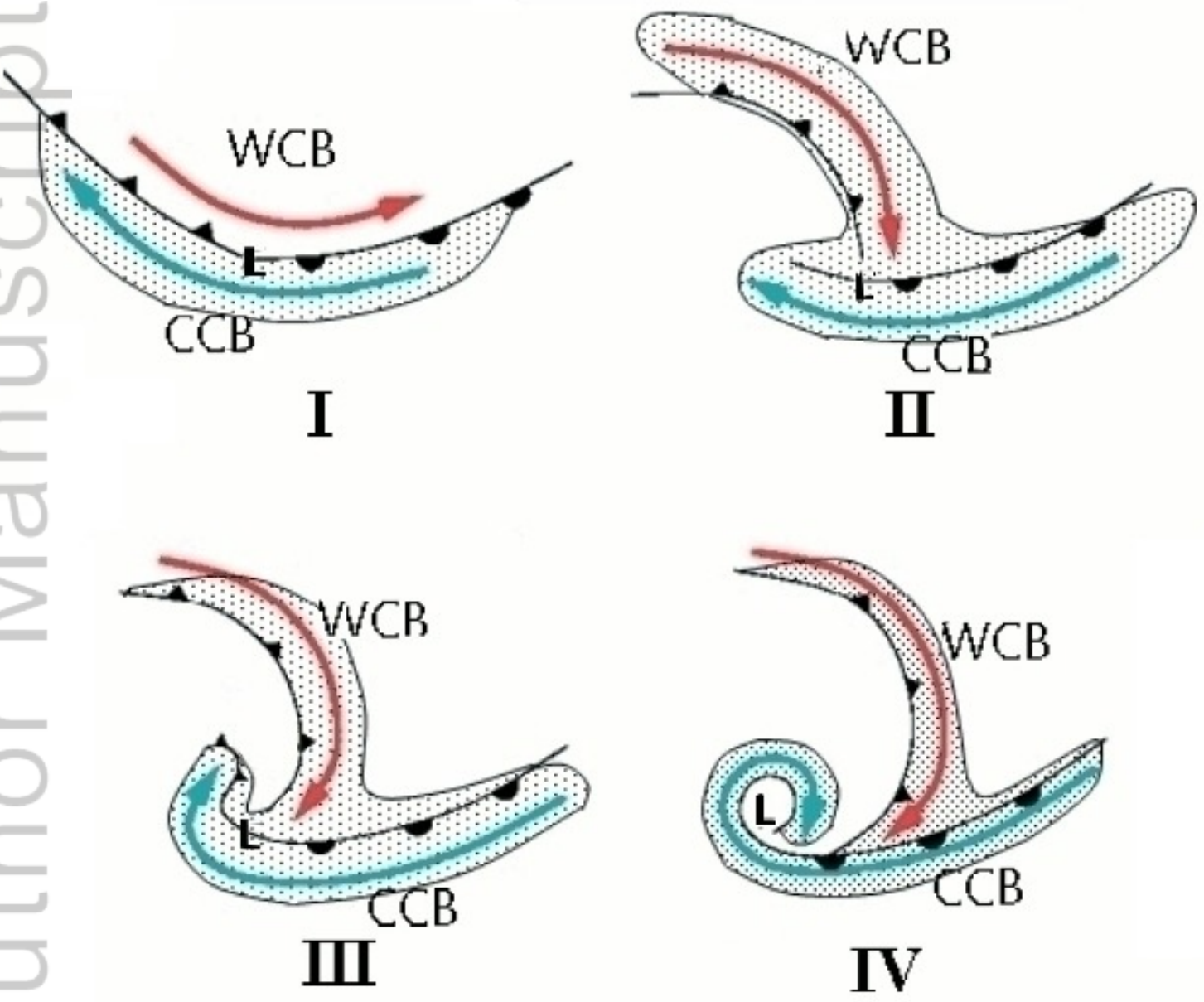

Fig1.jpeg

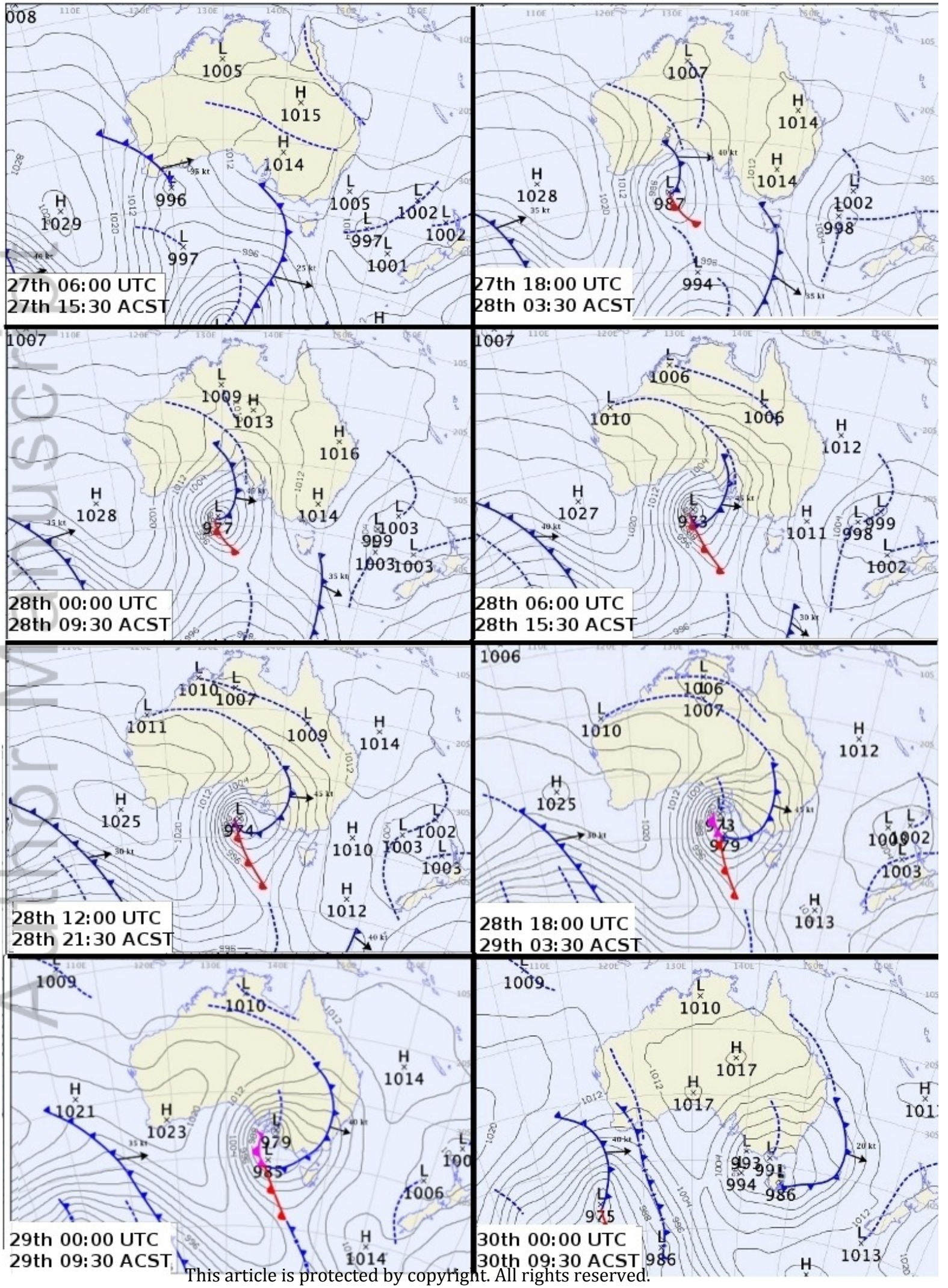

Fig2.jpeg

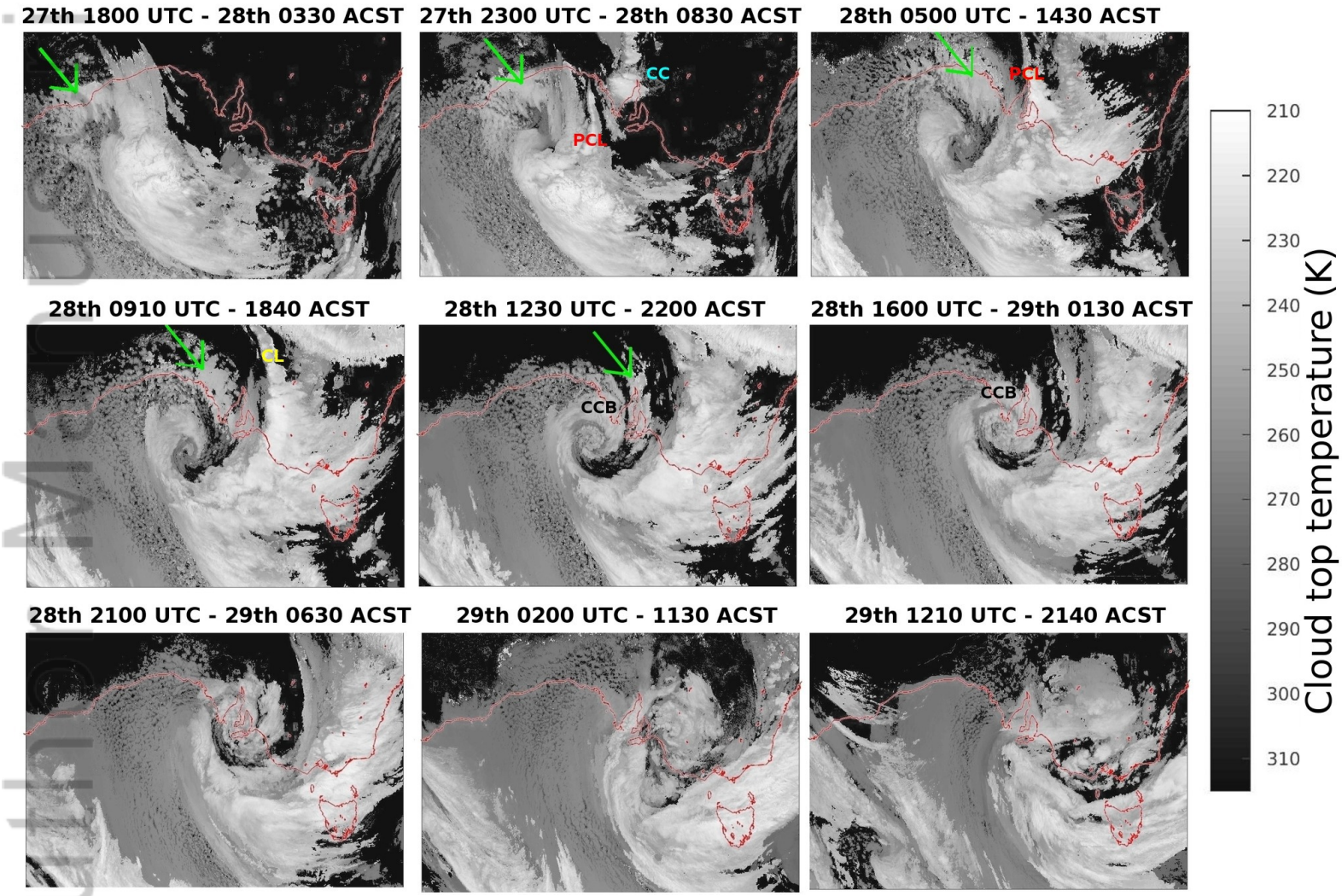

Fig3.jpeg

16001 Woomera Aerodrome
16090 Coober Pedy Airport
16096 Roxby Downs
16097 Ernabella (Pukatja)
16098 Tarcoola Aero
17043 Oodnadatta Airport
17110 Leigh Creek Airport
17123 Moomba Airport
17126 Marree Aero
18012 Ceduna Amo
18083 Wudinna Aero
18106 Nullarbor
18115 Neptune Island
18116 Cleve Aerodrome
18120 Whyalla Aero
18191 Coulta (Coles Point)
18192 Port Lincoln
18195 Minnipa Pirsa
18200 Thevenard Wind
18201 Port Augusta Aero
20062 Yunta Airstrip
21131 Clare High School
21133 Snowtown (Rayville Park)
21139 Port Pirie Aerodrome Aws
22031 Minlaton Aero
22046 Edithburgh
22049 Stenhouse Bay
22050 Kadina Aws
22053 Moonta (Warburto Point)
22803 Cape Willoughby
22823 Cape Borda
22841 Kingscote Aero
22843 Parndana Cfs Aws
23013 Parafield Airport
23034 Adelaide Airport
23052 Outer Harbour (Black Pole)
23083 Edinburgh Raaf
23090 Adelaide (Kent Town)
23109 Adelaide Airport (South West)
23122 Roseworthy Aws
23123 Adelaide Airport (Northeast)
23124 Adelaide Airport (Northwest)
23373 Nuriootpa Pirsa
23842 Mount Lofty
23875 Parawa West
23878 Mount Crawford Aws
23885 Noarlunga
23886 Sellicks Hill
23887 Kuitpo Forest Reserve
24024 Loxton Research Centre
24048 Renmark Aero
24580 Strathalbyn Racecourse
24584 Murray Bridge
25557 Keith (Munkora)
25562 Lameroo (Austin Plains)
26021 Mount Gambier Aero
26091 Coonawarra
26095 Cape Jaffa (The Limestone)
26099 Naracoorte Aerodrome
26100 Padthaway South
26105 Robe Airfield

Fig4.jpeg

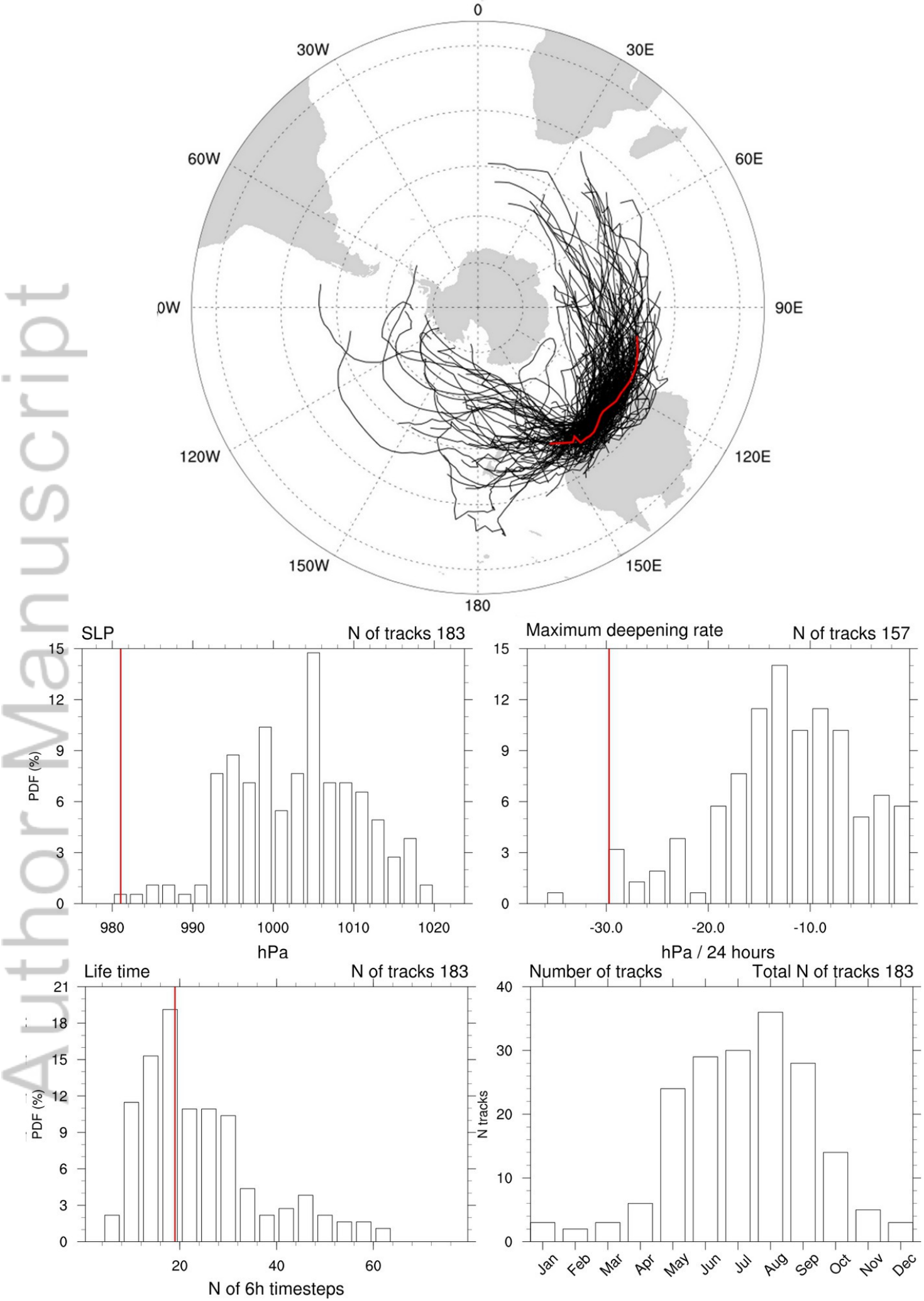

Fig5.jpeg

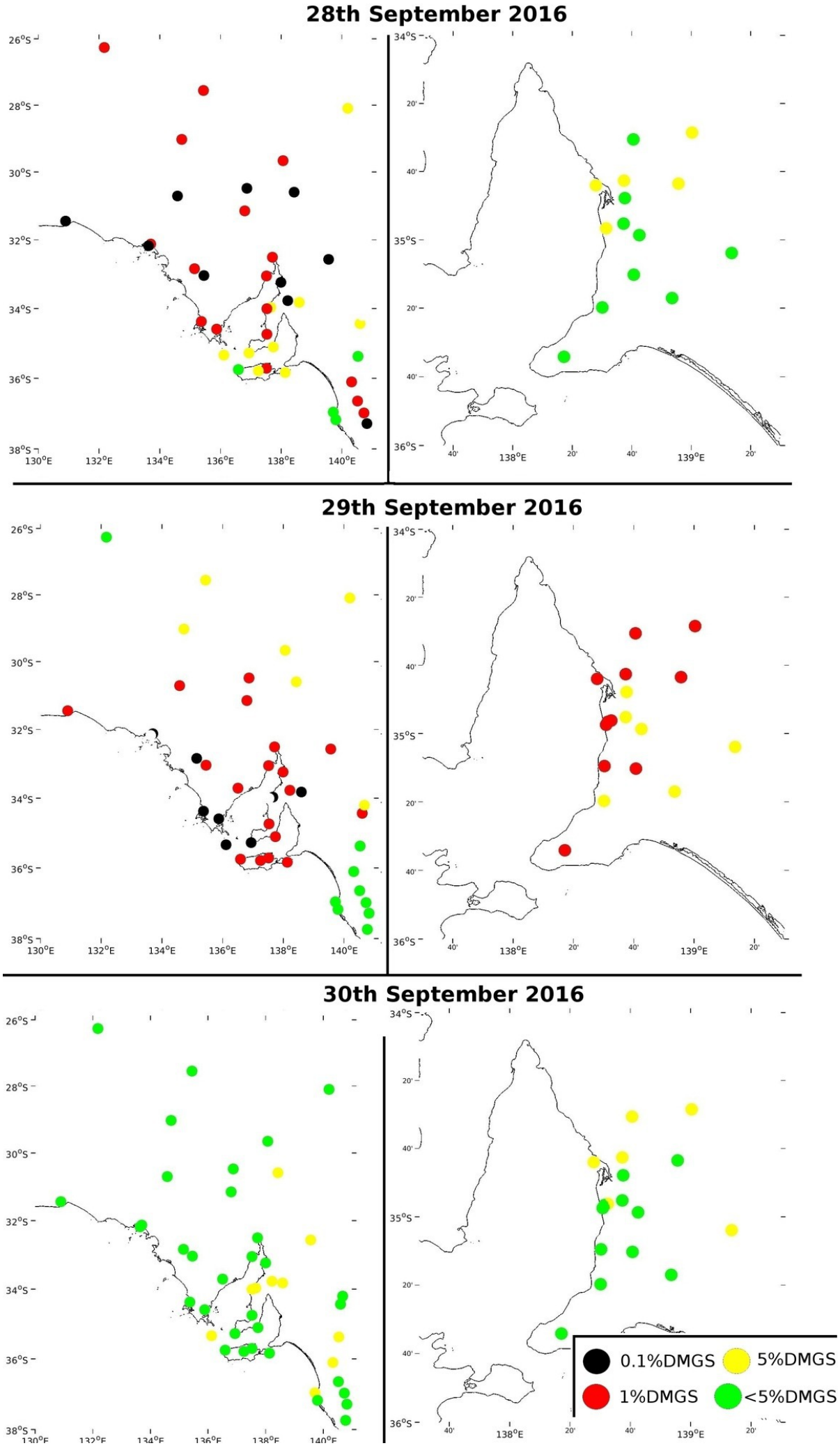

Fig6.jpeg

Dear Dr. Earl,

Your manuscript has been reviewed and the comments of the reviewers may be found at the foot of this message. They have recommended publication after some revisions have been made. Accordingly, I invite you to respond to the comments and revise your manuscript.

You have 90 days to submit your revised paper, after which the online submission system will block its upload. If you need more time please contact weather@wiley.com. However, it would be much appreciated if your revision could reach us well before the 90 days are up.

You can upload your revised manuscript and submit it through your Author Centre. Log into https://protect-au.mimecast.com/s/x3M0CANZ0ohRMKJxIGlj5j?domain=mc.manuscriptcentral.com and enter your Author Centre, where you will find your manuscript title listed under "Manuscripts with Decisions".

When submitting your revised manuscript, you will be able to respond to the comments made by the reviewers in the space provided. You can use this space to document the changes you make to the original manuscript.

IMPORTANT: Please make sure you closely follow the instructions for acceptable files. When uploading your revised manuscript, please delete the file(s) that you wish to replace and then upload the revised file(s).

Once again, thank you for submitting your manuscript to Weather. I look forward to receiving your revision.

Yours sincerely,

Jim Galvin

rmetseditorialoffice@wiley.com

Dear Jim,

Thank you for your email and the comments of the Reviewers on our two submissions. We are grateful to you and reviewers for the very positive remarks on our work and also appreciate the positive responses to the way we've split the manuscript.

We draw your attention to the point raised by reviewer 2 as to whether the Table should be placed in the main document, or located in a Supplementary Material section. As we point out below we feel that the Table represents an important component of the paper, and hence belongs in the main text. However, if you feel it would be better placed in Supplementary Material we would be quite happy to have it so-located.

Review: 1

Comments to the Author

Thank you. A worthwhile subject, well researched and presented. A few relatively minor matters require your attention, as listed below.

We greatly appreciate the positive views on our work made by the reviewer and have addressed each of the comments below.

Figure 3 as presented with this proof does not have the green arrow or other annotations mentioned in the text and figure description. However, these do exist on the (same) figure 3 presented with Part II.

Many thanks for noticing this. We have taken the reviewer's and editor's advice and included the annotations and taken the similar figure out of part 2.

Figure 3 would be better served with UTC time stamps as well, as in Figure 2. The text reference is otherwise that much more difficult to match with the frames.

Good point, these have been added

Line no. (pdf version line numbers)

14 acronym ETC not expanded at first use (necessary in the abstract?)

Well spotted, many thanks

90 insert 'sting jet' before the abbreviation '(SJ)'

Thanks, this has been added in

101 SJ is a plural here, 'SJs'?

Yes, many thanks

127 23hPa/24 contradicts 21.2hPa/24 in line 199

Thanks for alerting us to this apparent contradiction. '(according to the BoM)' has been added to line 127 and 'Our tracking analysis shows that' to line 199 for clarity.

156 acronym ERA not expanded at first use, here.

Thanks, 'European Centre for Medium-Range Weather Forecasts Reanalysis has been added

177 add after ...length of... : ...record at...

Thank you

182/3 surely DMGSs are wind speeds too? Suggest inserting 'average' or 'background' before the word windspeeds (which is properly two words anyway!)

Your suggestion makes a lot of sense. We have added 'absolute wind speeds' to make this clearer

209 gust should be plural

Yes, thanks for this

Review: 2

Comments to the Author

This all looks good, is interesting for weather readers and is well written. The only possible caveat is whether publication of the large table 1 is really necessary for this paper.

Many thanks for this comment. We originally had this table in the supplementary material; however a previous reviewer suggested that it's worth adding to the main document as we refer to it many times. We'll leave it up to the editor for a final decision on this. However we feel it is of value to be placed the main document.

Author/s:
Earl, N; Simmonds, I; Rudeva, I

Title:
Sub-synoptic scale features associated with extreme surface gusts during the South Australia Storm of September 2016-Part I: characteristics of the event

Date:
2019-08-01

Citation:
Earl, N., Simmonds, I. & Rudeva, I. (2019). Sub-synoptic scale features associated with extreme surface gusts during the South Australia Storm of September 2016-Part I: characteristics of the event. WEATHER, 74 (8), pp.278-285. https://doi.org/10.1002/wea.3385.

Persistent Link:
http://hdl.handle.net/11343/284759

File Description:
Accepted version